JACS
JOURNAL OF THE AMERICAN CHEMICAL SOCIETY
Article
pubs.acs.org/JACS

Probing the Limits of Alkaline Earth−Transition Metal Bonding: An Experimental and Computational Study

Matthew P. Blake,[†] Nikolas Kaltsoyannis,*[,‡] and Philip Mountford*[,†]

[†]Chemistry Research Laboratory, Department of Chemistry, University of Oxford, Mansfield Road, Oxford OX1 3TA, United Kingdom

[‡]Department of Chemistry, Christopher Ingold Laboratories, University College London, 20 Gordon Street, London WC1H 0AJ, United Kingdom

Supporting Information

ABSTRACT: Reduction of Fp_2 (Fp = $CpFe(CO)_2$) or $[Co(CO)_3(PCy_3)]_2$ (**15**) with Mg-mercury amalgam gave $[Mg\{TM(L)\}_2(THF)]_2$ (TM(L) = Fp or $Co(CO)_3(PCy_3)$ (**19**)) in which the TM is bonded to two Mg atoms. Reduction of **15** with Ca-, Sr-, Ba-, Yb-, Eu- and Sm-mercury amalgam gave a series of compounds "$M\{Co(CO)_3(PCy_3)\}_2(THF)_n$" (M = Ae or Ln) in which the M−Co bonding varies with the charge-to-size ratio of M. For M = Ca or Yb (**24**), each metal forms one M−Co bond and one M(μ-OC)Co η^1-isocarbonyl linkage. With M = Sr (**21**) or Eu (**25**), a switch from M−Co bonding to side-on (η^2) CO ligand coordination is found. $Sm^{II}\{Co(CO)_3(PCy_3)\}_2(THF)_3$ disproportionates in pentane to form $Sm^{III}\{Co(CO)_3(PCy_3)\}_3(THF)_3$ containing two Sm^{III}−Co bonds, in contrast with **25**, showing the importance of the Ln charge on Ln−TM bonding. Diffusion NMR spectroscopy found that in solution, **21** and **24** are dimeric compounds $[M\{Co(CO)_3(PCy_3)\}_2(THF)_3]_2$ that, according to DFT calculations, contain either one (Ae = Ca) or two (Ae = Sr) Ae−Co bonds per Co atom. DFT calculations in combination with Ziegler Rauk energy decomposition and atoms in molecules analysis were used to assess the nature and energy of Ae−Co bonding in a series of model compounds. The Ae−Co interaction energies decrease from Be to Sr, and toward the bottom of the group, side-on (η^2) CO ligand coordination competes with Ae−Co bonding. The PCy_3 ligand plays a pivotal role by increasing solubility in nondonor solvents and the Ae−Co interaction energy.

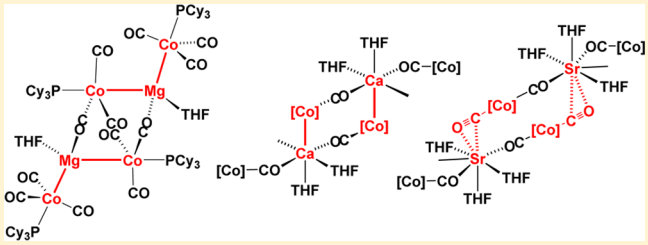

INTRODUCTION

The synthesis, structure, bonding, and reactivity of molecular compounds containing metal−metal bonds[1] has undergone a renaissance during the past decade or so. Reports of zinc−zinc[2] and magnesium−magnesium[3] single bonds, transition metal quintuple bonds,[1a,4] and the emergence of a body of 4f element− and 5f element−main group and transition metal bond partners highlight the intense interest in this field.[5−8] One of the remaining underdeveloped areas[3a] of this chemistry centers around the group 2 (alkaline earth, Ae) elements, which are among the most electropositive in the periodic table. For example, although Mg^I−Mg^I bonded dimers of the type $[(^RNacNac)Mg]_2$ (^RNacNac = $HC\{C(Me)NR\}_2$) and their analogues have been prepared and intensely studied since 2007,[3] no homobimetallic compounds with bonds between other Ae elements have been reported, despite a significant synthetic effort[9] and a number of computational studies on various model compounds of the type $[(L_x)Ae]_2$ (L_x = monoanionic ligand or ligand set).[10]

Heterobimetallic molecular compounds of the Ae elements in their 2+ oxidation state have been reported during the past few years; in particular, in the case of certain post-transition metals, specifically Ga, Ge, and Sn, as illustrated in Figure 1 and summarized in our recent review.[3a] These are relatively few in number, but they do include some examples with bonds involving both Mg and also the heavier congeners (Ca, Sr, and Ba).

In contrast, the boundaries and limits of alkaline earth−transition metal (Ae−TM) bonding are far from being satisfactorily established. Since the 1970s, there have been occasional reports of structurally authenticated compounds with Ae−TM bonds (e.g., **1**−**3**, Figure 2), but until very recently, these involved only magnesium.[11] The first Be−TM bonded compounds (**4**) were described in 2009,[12] and to date, only a single example of a Ca−TM bond has been communicated: namely, $[CaFp_2(THF)_3]_2$ (**5**).[13] Along with its ytterbium analogue (**6**), this also allowed the first structural and electronic structure comparison (in the context of metal−metal bonding) between a pair of similarly sized Ae(II) and Ln(II) elements.

Our attempts to prepare a magnesium analogue of **5** and **6** were unsuccessful and gave only the isocarbonyl-bridged complex $MgFp_2(THF)_4$ (**8**) without any Mg−Fe bonds.[13] On the other hand, whereas reaction of $Mg(^{Dipp}NacNac)I(THF)$ with KFp in THF gave $Mg(^{Dipp}NacNac)Fp(THF)$ (**7**, Figure 2)

Received: July 27, 2015
Published: September 4, 2015

DOI: 10.1021/jacs.5b07866
J. Am. Chem. Soc. 2015, 137, 12352−12368

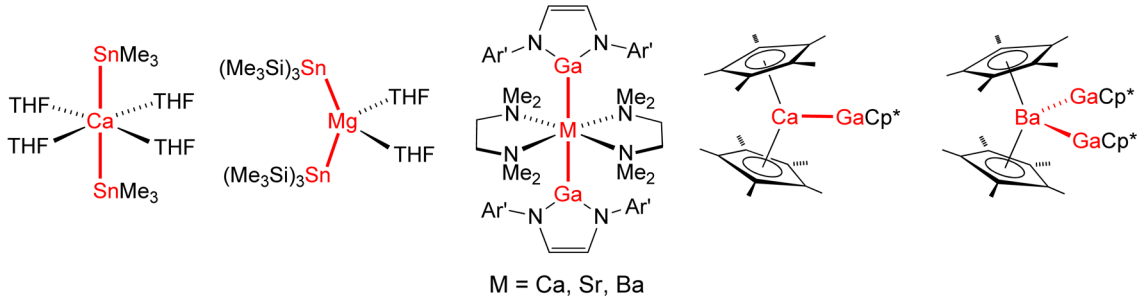

Figure 1. Examples of compounds with bonds between Ae metals and post-transition metals (Ar′ = Dipp).[3a]

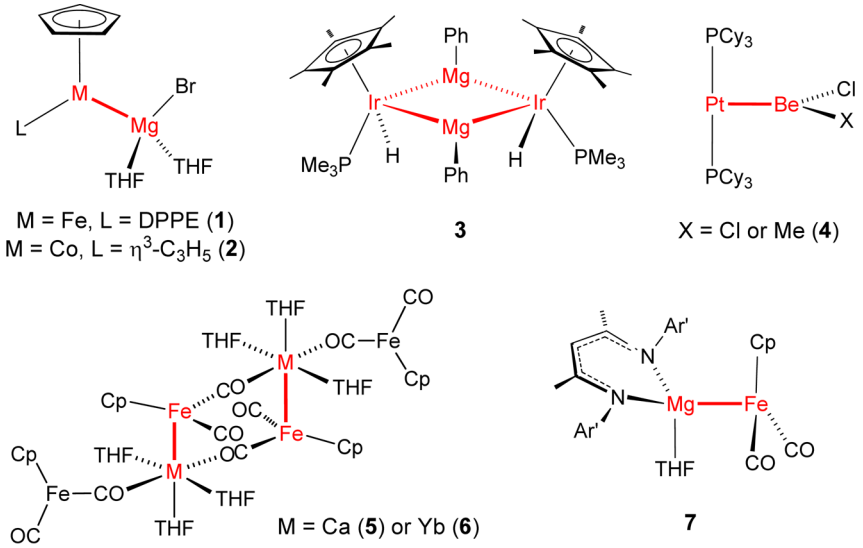

Figure 2. Examples of compounds with bonds between Ae metals and transition metals (Ar′ = Dipp).

with a Mg−Fe bond, the corresponding reactions starting from $[M(^{Dipp}NacNac)I(THF)]_2$ (M = Ca or Yb) gave dimeric $[M(^{Dipp}NacNac)(\mu\text{-Fp})\ (THF)]_2$ with only M(μ-OC)Fe isocarbonyl linkages (Dipp = 2,6-$C_6H_3{}^iPr_2$).[11b] Therefore, although compound **5** has established the precedent for the possibility of bonding between the heavier Ae elements and the transition metals, there was not yet in the literature any sort of coherent picture of Ae−TM bonding in terms of periodic trends for self-consistent supporting ligand systems. It was not clear whether compounds containing Sr−TM or Ba−TM bonds could be isolated; what the characteristics of such bonds would be; and what, if any, structural relationships there would be between other pairs of Ae elements and their similarly sized divalent lanthanide counterparts (i.e., Ca^{II} vs Yb^{II} (as in **5** and **6**) and Sr^{II} vs Sm^{II} or Eu^{II}). In this paper, we report new comprehensive synthetic, structural, spectroscopic, and computational studies of Ae−TM bonded compounds with the aim of addressing these questions and mapping out the scope and limitations of the use of transition metal carbonylate anions in this regard.

RESULTS AND DISCUSSION

Scope and Selection of Transition Metal Anions for Ae−TM Bonds. Ae−TM bonds are significantly ionic, and therefore, the choice of transition metal anion $[(L_x)TM]^-$ for the Ae−TM bond pair must recognize this. The ligand set "(L_x)" and the transition metal must be able to accommodate the anionic charge transferred from the electropositive Ae. Examination of the structural literature[14] for other polar M−TM bond partners (i.e. where M = lanthanide (Ln) or actinide (An))[5a] or an early transition metal (in early late heterobimetallic compounds[15]) quickly reveals only a handful of apparently privileged anions in this context. These are $[CpM(CO)_2]^-$ (M = Fe ("Fp") or Ru ("Rp")); $[Co(CO)_4]^-$ and its monophosphine analogue $[Co(CO)_3(PR_3)]^-$; and, more recently (due to the contributions of Kempe[6a,c,e] and Liddle[8f,g]), $[Cp_2Re]^-$. The dianionic $[Fe(CO)_4]^{2-}$ has also found use in the attempted synthesis of M−TM bonds but has met with more limited success as a result of the onset of extensive isocarbonyl bonding.[6i,j,16] Bonds to carbonylate anions can be formed by either transmetalation (e.g., from NaFp) or reductive cleavage (e.g., of Fp_2 or $[Co(CO)_3(PR_3)]_2$) using a lower oxidation state $(L_x)M$ species or the metal itself. Bonds to Cp_2Re can also be formed by transmetalation from a salt of $[Cp_2Re]^-$,[6a,8f] or by alkane elimination using the moderately acidic hydride Cp_2ReH and a metal−alkyl precursor.[6c,e,8g]

The advantages and disadvantages of carbonylate vs noncarbonylate anions have been recognized in the literature, and amount to a *Catch-22* scenario.[5a,17] Carbonylate anions stabilize very well the negative charge build-up upon forming the polar M−TM bond through π back-donation to the carbonyl ligands, but often M−(μ-OC)−TM bridges are formed in preference to the target metal−metal bond. Kempe has recently summarized this as "the isocarbonyl problem,"[5a] which Marks also noted in the context of synthesizing An−TM bonds.[8j] On the other hand, the $(L_x)M-ReCp_2$ moiety, particularly for the electropositive lanthanides, is rather prone

DOI: 10.1021/jacs.5b07866
J. Am. Chem. Soc. 2015, 137, 12352−12368

Scheme 1. Synthesis of $MgFp_2(THF)_4$ (8) and $[MgFp_2(THF)]_2$ (9)

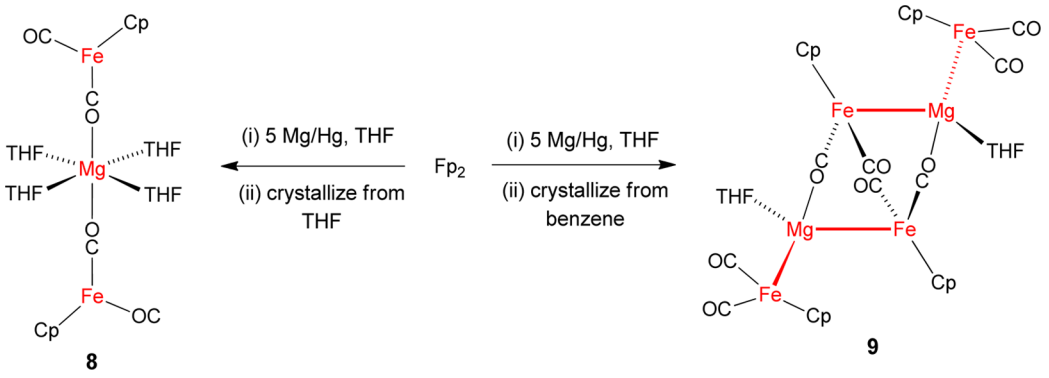

to intramolecular deprotonation and Cp ligand C−H activation decomposition pathways.[6b,c,18]

In choosing which class of anion to employ in our search for new Ae−TM bonds, we noted in particular that the heavier Ae element−alkyl bonds are considerably more reactive and prone to degradation than those of their Mg−alkyl (Grignard) counterparts,[9d,19] so we were concerned that Ae−TM bonds would likewise be prone to unfavorable side reactions. In addition, whereas heteroleptic precursors of the type $(L_x)Ae-X$ (X = halide, amide, or alkyl; L_x = monoanionic supporting ligand) are well-established for the lighter Ae elements, for Ca, Sr, and Ba, enforcement of such mixed-ligand environments becomes more problematic. Furthermore, prior to our own work, several mid- to late-lanthanides in their 2+ and 3+ oxidation states had been found to form Ln−Fe or Ln−Ru bonds (Ln = Nd^{III},[6f] Yb^{II},[6d,i,j] or Lu^{III}[6h]) using Fp^-, Rp^-, and $[Fe(CO)_4]^{2-}$ anions. Encouraged by these results and our initial success with the synthesis of $[MFp_2(THF)_3]_2$ (M = Ca (**5**) or Yb (**6**)),[13] we set out to explore the potential for Ae−TM bonding using a range of these carbonylate anions.

Compounds with Group 8 Carbonylate Anions. *Magnesium.* In our preliminary communication,[13] we found that reduction of Fp_2 with an excess of Ca/Hg amalgam in THF, followed by crystallization from the same solvent, gave $[CaFp_2(THF)_3]_2$ (**5**) with one Ca−Fe bond per Ca center, whereas with Mg/Hg, the analogous reaction gave $MgFp_2(THF)_4$ (**8**, Scheme 1, no Mg−Fe bond). The solution IR spectrum of **8** in THF was characteristic of such an isocarbonyl-bridged species with ν(CO) = 1875 cm^{-1} for the terminal carbonyl ligands and ν(CO) = 1703 cm^{-1} for the bridging ones. The latter engage in enhanced $Fe(d_\pi) \rightarrow CO(\pi^*)$ back-bonding as judged by shorter Fe−CO and longer Fe−C≡O bonds. DFT calculations, on the other hand, found that Mg−Fe bonds are stronger than Ca−Fe ones, and we rationalized the difference in structure between **8** and its Ca and Yb counterparts as being due to the higher charge density of Mg^{2+} favoring THF coordination and thus (by implication) leading to the formation of isocarbonyl bridges in place of Mg−Fe bonds.

Interestingly, the bulk material obtained *prior* to crystallization from THF has the overall composition "$MgFp_2(THF)_{1.6}$" and a significantly different IR spectrum in the solid state (Nujol mull: ν(CO) = 1912, 1855, and 1775 cm^{-1}). Although this material is poorly soluble in nondonor solvents, we recently obtained diffraction-quality crystals of $[MgFp_2(THF)]_2$ (**9**, Scheme 1) from a dilute benzene solution layered with pentane. The solid state structure is shown in Figure 3 along with key bond distances and angles. A similar

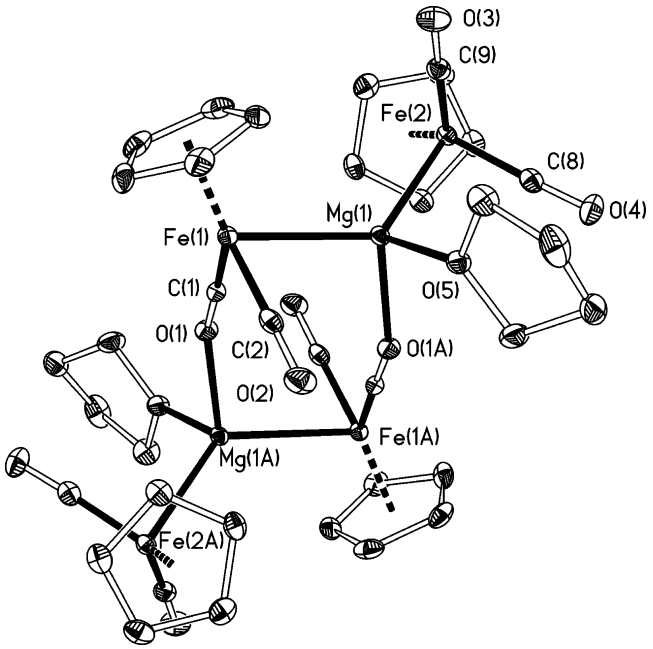

Figure 3. Displacement ellipsoid plot of $[MgFp_2(THF)]_2$ (**9**). H atoms omitted. Selected distances (Å) and angles (°): Mg(1)−Fe(1), 2.6112(5); Mg(1)−Fe(2), 2.5629(5); Mg(1)−O(1A), 2.1015(11); Mg(1)−O(5), 2.0479(11); Fe(1)−Mg(1)−Fe(2), 128.70(2); Fe(1)−C(1), 1.7016(14); Fe(1)−C(2), 1.7395(16); C(1)−O(1), 1.195(2); C(2)−O(2), 1.164(2).

material, "$MgFp_2(THF)_2$", was reported by McVicker some time ago, with a similar IR spectrum but no structural characterization.[20] The solid state structure is consistent with the IR data, which imply a mixture of terminal and bridging carbonyl ligands.

In the solid state, compound **9** is a centrosymmetric dimer with two equivalent $MgFp_2(THF)$ moieties connected by a pair of $Mg(\mu$-OC)Fe isocarbonyl linkages that, together with a pair of Mg−Fe bonds, form part of a central eight-membered ring. The geometry at Mg(1) is approximately tetrahedral. Compound **9** is the first example of a compound in which an Ae element uses both of its valencies to bond to two transition metals (see also the cobalt analogue described below). The Mg(1)−Fe(1) and Mg(1)−Fe(2) distances of 2.6112(5) and 2.5629(5) Å, respectively, are comparable to those for $Mg(^{Dipp}NacNac)Fp(THF)$ (2.6326(4) Å)[11b] and CpFe(DPPE)$MgBr(THF)_2$ (2.593(7) Å),[11j] the only two previous examples containing Mg−Fe bonds. The significant difference

DOI: 10.1021/jacs.5b07866
J. Am. Chem. Soc. 2015, 137, 12352−12368

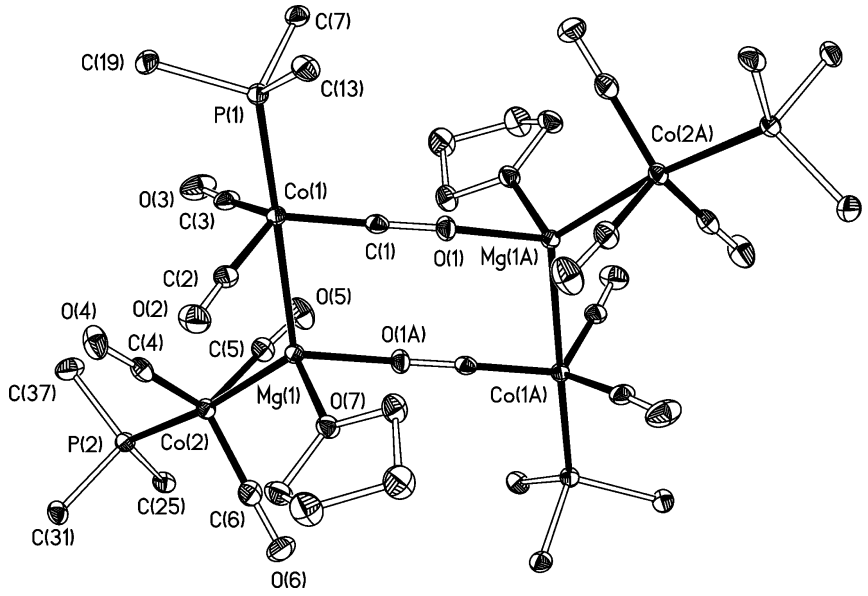

Figure 4. Displacement ellipsoid plot of $[Mg\{Co(CO)_3(PCy_3)\}_2(THF)]_2$ (**19**). H atoms and cyclohexyl methylene carbon atoms omitted. Selected distances (Å) and angles (°): Mg(1)−Co(1), 2.6163(6); Mg(1)−Co(2), 2.5427(6); Mg(1)−O(1A), 2.0390(14); Mg(1)−O(7), 2.0335(14); Co(1)−Mg(1)−Co(2), 124.34(2); sum of OC−Co(1)−P(1), 300.9(2); sum of OC−Co(2)−P(2), 303.2(2).

of 0.0483(1) Å between the Mg(1)−Fe(1,2) bond lengths in **9** implies that Fe(1) is a poorer donor. This may be because of its stronger back-bonding to the μ-CO ligand (cf. Fe(1)−C(1) = 1.7016(14) vs Fe(1)−C(2) = 1.7395(16); Fe(2)−C(8,9) (av) = 1.7319 (11) Å). The central eight-membered ring motif in **9** is analogous to that in **5**, which also contains alternating Ae−TM bonds and isocarbonyl linkages.

The differing structures found for **5**, **8**, and **9** points to the importance of matching the supporting ligand (which may also be derived from the solvent) environment to the requirements of the particular Ae−TM (or Ln−TM) bond. As a further example of the influence of ligand type, we found that treatment of $MgFp_2(THF)_4$ (**8**) with 4 equiv of HMPA gave the separated ion pair salt $[Mg(HMPA)_4][Fp]_2$ (**10**) with ejection of both carbonylate anions from the coordination sphere. The solid state structure of $[Mg(HMPA)_4]^{2+}$ and one of the $[Fp]^-$ anions is shown in Figure S1 of the SI. In contrast, the homologous calcium and ytterbium compounds with the same Ae/HMPA ratio were found to adopt six-coordinate complexes $MFp_2(HMPA)_4$ (M = Ca (**11**) or Yb (**12**)) in solution (as judged by NMR and IR spectroscopy) and in the solid state (Figure S2 of the SI for **12**). The differing structures of **8**, **9**, and **10** provide a qualitative measure of the relative strength of the different Mg−ligand interactions for Fp, THF, and HMPA.

Compound **10** is the first time that the "free" parent Fp^- anion has been crystallographically characterized, previous structures being for Na^+ or K^+ counterions having significant interactions with the carbonyl ligands.[21] The IR spectra for **10** in the solid state (Nujol mull: ν(CO) = 1863 and 1789 cm^{-1}) and THF solution (ν(CO) = 1865 and 1787 cm^{-1}) are effectively identical and also the same as those for KFp (1865 and 1788 cm^{-1}) and NaFp (1862 and 1786 cm^{-1}) in THF in the presence of crown ethers, proposed to exist as solvent-separated ion pairs under these conditions.[22]

Strontium. In an analogous manner to the synthesis of **5** and **9**, reduction of Fp_2 in THF with an excess of Sr/Hg amalgam was carried out. This afforded an extremely air- and moisture-sensitive, orange solid tentatively assigned as "$SrFp_2$" (**13**) which was stable in THF, THF-d_8, or pyridine-d_5 solution (solutions in the latter solvent showed no residual THF). It was not possible to grow diffraction-quality crystals or to obtain consistent elemental analyses. The ^1H and $^{13}C\{^1H\}$ NMR data showed just one species, but although the IR data in the solid state (Nujol: ν(CO) = 1871, 1808, and 1749 cm^{-1}) were broadly comparable to the corresponding data for the magnesium and calcium counterparts, no meaningful conclusion could be drawn from these regarding the presence or absence of Sr−Fe bonding. The IR spectrum in THF solution showed two bands with ν(CO) = 1878 and 1712 cm^{-1}. These are also analogous to those for **5** and **9** in THF solution, suggesting the presence of a species of the type $SrFp_2(THF)_n$ ($n \geq 4$) with isocarbonyl bridges.

Other Group 8 Carbonylate Anions. We targeted two additional group 8 anions, $[CpRu(CO)_2]^-$ (Rp^-) and $[Fe(CO)_4]^{2-}$, focusing on calcium as an intermediate-sized group 2 element. Unfortunately, we were unable to isolate Ca−TM products from these reactions. A number of otherwise interesting X-ray structures were obtained (Figures S3−S7 of the SI); further details are given in the Supporting Information. It is clear that further development of Ae−TM structure and bonding will not be easily achievable with these group 8 carbonylate anions.

Ae Compounds with $[Co(CO)_3(PR_3)]^-$ (R = Ph or Cy) Ligands. A large number of heterobimetallic compounds based on the $[Co(CO)_3(L)]^-$ and related anions (L = CO or PR_3) have been structurally authenticated[14] for both the transition and post-transition metals. In contrast, examples have only very recently been reported for the actinides.[8a−c] No examples of Ln−Co bonds are known, although separated ion pairs based on $[Co(CO)_4]^-$ and isocarbonyl-bridged isomers are well-established.[14,16] One report of Ae−Co bonding was published in 1986[11f] in which CpCo(η-C_3H_5)MgBr(THF)$_2$ and CpCo(η-C_2H_4)(μ-Ph)MgBr(TMEDA) were prepared from [CpCo(η-C_2H_4)$_2$] and a Grignard reagent. We considered $[Co(CO)_3(L)]^-$ a potentially useful probe of Ae−Co (and also

DOI: 10.1021/jacs.5b07866
J. Am. Chem. Soc. 2015, 137, 12352−12368

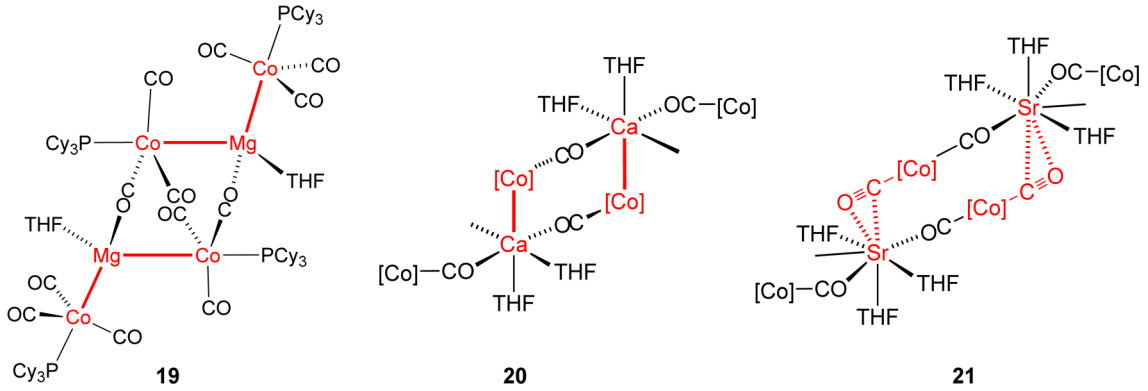

Figure 5. Schematic comparison of the key features of "Ae{Co(CO)$_3$(PCy$_3$)}$_2$(THF)$_n$" (n = 1 (Mg), 2 (Ca), or 3 (Sr)). [Co] = Co(CO)$_2$(PCy$_3$) for **20** and Co(CO)$_n$(PCy$_3$) (n = 1 or 2) for **21**.

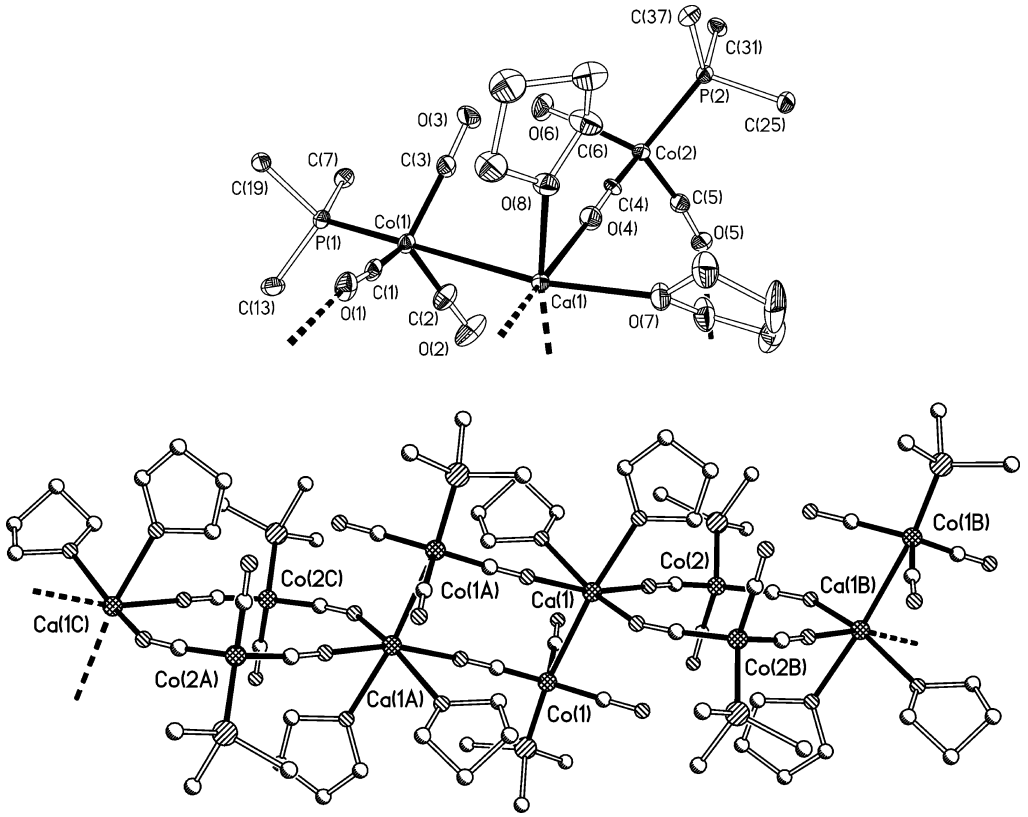

Figure 6. Displacement ellipsoid plot of the asymmetric unit (top) and ball and stick plot (bottom) of a portion of the infinite chain of [Ca{Co(CO)$_3$(PCy$_3$)}$_2$(THF)$_2$]$_\infty$ (**20**). H atoms and cyclohexyl methylene groups omitted. Selected distances (Å) and angles (°): Ca(1)–Co(1), 3.0450(9); Ca(1)–O(4), 2.344(3); Ca(1)–O(7), 2.400(3); Ca(1)–O(8), 2.366(3); C(4)–Co(2)–C(5), 108.46(17); sum of OC–Co(1)–P(1), 305.8(3); sum of OC–Co(2)–P(2), 327.4(4).

Ln–Co) bonding because of the opportunity to control solubility in nondonor solvents by correct choice of the ligand, L. It has also been shown that the donor ability of [Co(CO)$_3$(L)]$^-$ both to metal centers and to hydrogen bond donors R$_3$NH$^+$ can be improved by using a more strongly σ-donating phosphine as L in place of CO.[15b,23]

Magnesium, Calcium, and Strontium. We initially assessed three cobalt compounds: [Co(CO)$_4$]$_2$, [Co(CO)$_3$(PPh$_3$)]$_2$ (**14**), and [Co(CO)$_3$(PCy$_3$)]$_2$ (**15**). Reduction of [Co(CO)$_4$]$_2$ or **14** with Mg/Hg amalgam in THF gave insoluble materials that could not be characterized. [Co(CO)$_4$]$_2$ was not studied further. Reduction of **14** with Ca/Hg, Sr/Hg, or Ba/Hg amalgams in THF afforded the homologous series Ca{Co(CO)$_3$(PPh$_3$)}$_2$(THF)$_4$ (**16**), [Sr{Co(CO)$_3$(PPh$_3$)}$_2$(THF)$_5$]$_2$ (**17**), and [Ba{Co(CO)$_3$(PPh$_3$)}$_2$(THF)$_6$]$_2$ (**18**) in 71–89% yields. All were insoluble in nondonor solvents but could be crystallized from THF. The solid state structures of **16**–**18** (Figures S8–S10 of the SI) show that none possesses an Ae–Co bond, and only Ae(μ-OC)Co isocarbonyl linkages are observed.

In contrast, reduction of **15** with Mg/Hg amalgam in THF afforded [Mg{Co(CO)$_3$(PCy$_3$)}$_2$(THF)]$_2$ (**19**) as a toluene-soluble, white solid in 87% isolated yield. The solid state structure is shown in Figure 4, and schematic representations of the structure of **19** and its Ca and Sr congeners are illustrated in Figure 5. Centrosymmetric **19** is dimeric in the solid state with

DOI: 10.1021/jacs.5b07866
J. Am. Chem. Soc. 2015, 137, 12352–12368

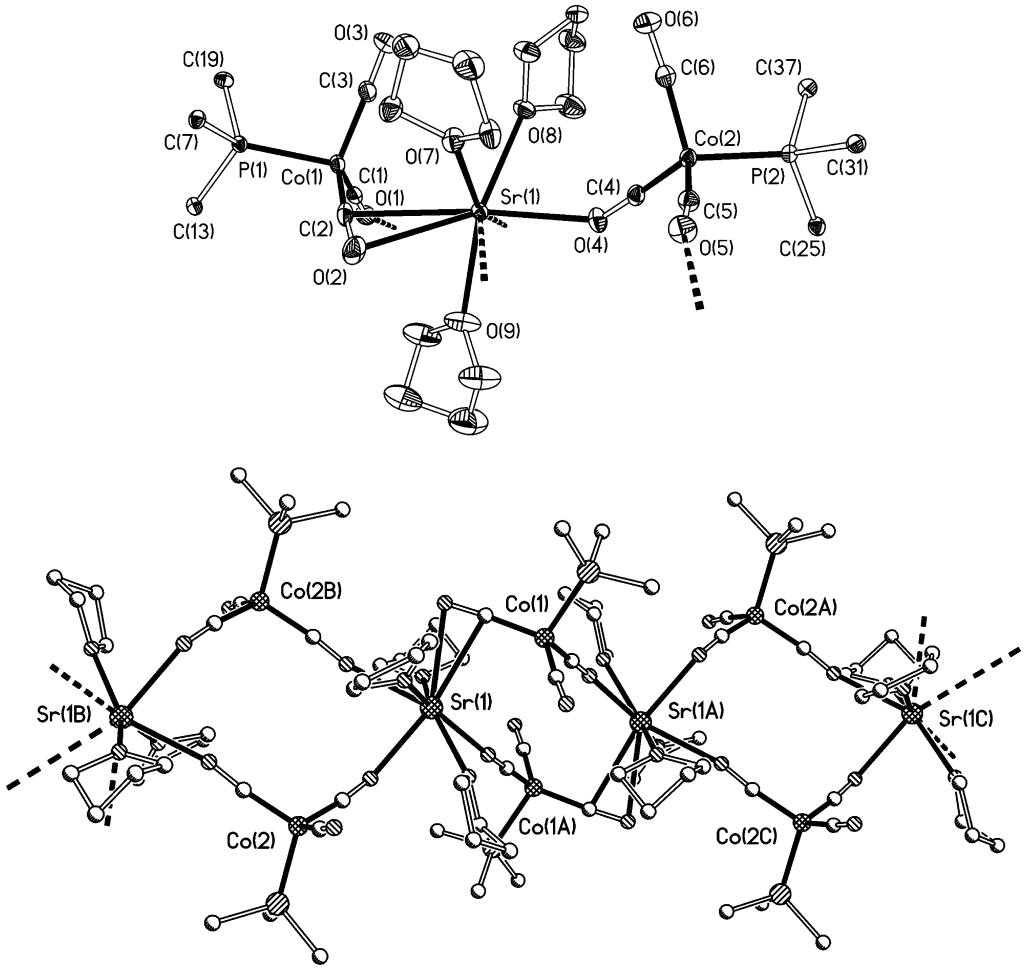

Figure 7. Displacement ellipsoid plot of the asymmetric unit (top) and ball and stick plot (bottom) of a portion of the infinite chain of $[Sr\{Co(CO)_3(PCy_3)\}_2(THF)_3]_\infty$ (**21**). H atoms and cyclohexyl methylene carbon atoms omitted. Selected distances (Å) and angles (°) Sr(1)···Co(1), 3.6263(4); Sr(1)−C(2), 2.909(2); Sr(1)−O(2), 2.879(2); Sr(1)−O(4), 2.5639(18); Sr(1)−O(7), 2.5401(18); Sr(1)−O(8), 2.5520(17); Sr(1)−O(9), 2.559(2); sum of OC−Co(1)−P(1), 311.1(3); sum of OC−Co(2)−P(2), 326.9(3).

two $Mg\{Co(CO)_3(PCy_3)\}_2(THF)$ units connected by isocarbonyl linkages. Each approximately tetrahedral Mg is directly bonded to two Co atoms, a THF ligand, and the oxygen of a μ-isocarbonyl ligand.

Together with $[MgFp_2(THF)]_2$ (**9**), **19** is the first example of a compound with two Ae−TM bonds per Ae metal center, although this is not uncommon for Ae−post-transition metal complexes.[7j,24] The Mg−Co bond distances of 2.6163(6) and 2.5427(6) Å are shorter than the sum of the Alvarez covalent radii (2.67 Å)[25] and comparable to those found for $CpCo(\eta\text{-}C_3H_5)MgBr(THF)_2$ (2.480(4) Å) and $CpCo(\eta\text{-}C_2H_4)(\mu\text{-}Ph)MgBr(TMEDA)$ (2.565(3) Å). The geometries at Co(1) and Co(2) are approximately trigonal bipyramidal, as expected with *trans*-axial coordination of the Mg(1) and P(1,2) atoms at Co(1,2), respectively. The central moiety of **19** is very similar to that in **9**: namely, an eight-membered ring containing the two Mg(μ-OC)Co linkages and two of the Mg−Co bonds. This structural unit, which is also found in **5**, **6** and $[Yb\{CpRu(CO)_2\}\}_2(THF)_2]_\infty$[6d] seems to be a common motif of both Ae−TM and Ln−TM bonded complexes in which carbonyl ligands are present. As was the case for **9**, the Mg−Co bond internal to the eight-membered ring (Mg(1)−Co(1) = 2.6163(6) Å) is longer than the external one (Mg(1)−Co(2) 2.5427(6) Å).

The sum of the R_3P−Co−CO angles $\sum$(P−Co−CO) in adducts of the type *trans*-$Co(CO)_3(PR_3)X$ has been proposed as a measure of the extent of Co−X interaction as the d^{10} $[Co(CO)_3(PR_3)]^-$ anion distorts from its relaxed tetrahedral geometry to favor Co−X bonding. For example: Me_3Sn−$Co(CO)_3(PPh_3)$, $\sum$(P−Co−CO) = 284°;[26] {MeSi(SiMe$_2$NTol)$_3$}M−$Co(CO)_3(PAr_3)$ (M = Ti or Zr), $\sum$(P−Co−CO) = 285 or 287°;[23a] {HC(SiMe$_2$NXyl)$_3$}U−$Co(CO)_3(PPh_3)$, $\sum$(P−Co−CO) = 297°;[8c] N(CH$_2$CH$_2$N)$_3$NH···$Co(CO)_3(PAr_3)$ (PAr_3 = PPh_3, $P(Ph)Tol_2$ or $PTol_3$), $\sum$(P−Co−CO) = 307−314°.[23b,27] The $\sum$(P−Co−CO) values in **19** (300.9(2) and 303.2(2)°) are generally larger than previously found for transition metal and post-transition metal complexes but substantially less than those in the N−H···Co hydrogen-bonded species.[23b,27] Note that the only relevant structurally characterized previous examples feature PAr_3 ligands (Ar = Ph or Tol). These have a Tolman cone angle[28] of 145°, whereas the PCy_3 ligand in **19** has a cone angle of 170°. For additional comparison, we also calculated (DFT) the structures of $[Co(CO)_3(PCy_3)]^-$ and $Co(CO)_3(PCy_3)H$ for which $\sum$(P−Co−CO) is 324.3 and 295.6°, respectively (Figure S11 of the SI).

Reaction of **15** with an excess of Ca/Hg amalgam in THF afforded a toluene-soluble product, **20**, of overall composition "$Ca\{Co(CO)_3(PCy_3)\}_2(THF)_2$" in 84% yield. In the solid state

DOI: 10.1021/jacs.5b07866
J. Am. Chem. Soc. 2015, 137, 12352−12368

(Figure 6), **20** forms an infinite chain consisting of eight- and 12-membered rings connected at their vertices by six-coordinate calcium atoms. Each calcium forms a Ca−Co bond, the length of which, 3.0450(9) Å, is again comparable to the sum of the covalent radii (3.02 Å). The eight-membered ring containing Co(1), Ca(1), Co(1A), and Ca(1A) is analogous to the corresponding motifs in **5**, **9**, and **19** and has two Ca−Co bonds and two Ca(μ-OC)Co linkages. The 12-membered ring containing Co(2), Ca(1), Co(2B), and C(1B) contains only Ca(μ-OC)Co isocarbonyl linkages. The sum of the OC−Co−P angles at the metal−metal bonded Co(1) atom ($\sum$(OC−Co(1)−P(1)) = 305.8(3)°)) is comparable to those in **19**, whereas for Co(2), $\sum$(OC−Co(2)−P(2)) = 327.4(4)°. This type of value may be taken as a reference point for a noninteracting cobalt center and is comparable to that calculated by DFT for $[Co(CO)_3(PCy_3)]^-$.

Reduction of **15** with Sr/Hg amalgam in THF afforded toluene-soluble **21** of composition "$Sr\{Co(CO)_3(PCy_3)\}_2(THF)_3$" in 70% yield. Crystallization from pentane gave the structure shown in Figure 7. Like **20**, in the solid state, **21** forms an infinite chain. The coordination environment at each Sr (Figure 7, top) is interesting, each being bound to three THFs; three η^1-O-bound isocarbonyl groups; and a side-on, η^2-bound CO ligand of Co(1) with Sr(1)−C(2) = 2.909(2) and Sr(1)−O(2) = 2.879(2) Å. Such side-on bonding of a ligand to an Ae element is extremely unusual. One relevant structurally characterized example from group 2 is Schumann's butenyl-substituted metallocene (η^5-,η^2-$C_5Me_4CH_2CH_2CH{=}CH_2)_2Sr$ in which the pendant alkene bonds to Sr with Sr···C distances in the range 2.99−3.25 Å.[29] The Sr(1)···Co(1) distance of 3.6263(4) Å in **21** is somewhat larger than the sum of the covalent radii (3.21 Å)[25] but may still indicate a residual weak interaction, with the sum of the OC−Co(1)−P(1) angles being 311.1(3)° (for the other cobalt center, $\sum$(OC−Co(2)−P(2)) = 326.9(1)°).

The infinite chain (Figure 7, bottom) consists of two types of $[Sr\{\mu\text{-}Co(CO)_3(PCy_3)\}_2Sr]$ rings. The 12-membered ring containing Sr(1), Sr(1B), Co(2), and Co(2B) is analogous to that in **20**. The other ring that contains Sr(1), Sr(1A), Co(1), and Co(1A) in a sort of "stretched" version of the eight-membered rings described above with the side-on carbonyl interaction to Sr(1) winning out over a shorter Sr(1)−Co(1) bond.

Diffusion NMR Spectroscopy. We used diffusion NMR spectroscopy to probe the solution structures of **19** and **21** (it was not possible to study **20** because of its low solubility in nondonor solvents at the necessary concentration). The results are shown in Table 1, together with comparative reference data for $[Co(CO)_3(PCy_3)]_2$ (**15**) and an ytterbium compound $[Yb\{Co(CO)_3(PCy_3)\}_2(THF)_3]_2$ (**24**) discussed later on.

The solution effective molecular volume of 1178 Å^3 for **19** is intermediate between that expected for dimeric $[Mg\{Co(CO)_3(PCy_3)\}_2(THF)]_2$ (1788 Å^3 based on the X-ray structure) and a monomer $Mg\{Co(CO)_3(PCy_3)\}_2(THF)$ (**19_mono**, estimated 868 Å^3). Assuming fast exchange between **19** and **19_mono** eq eq 1, as indicated by single sets of ^{1}H, ^{13}C, and ^{31}P NMR resonances, this suggests that **19** dissociates by ∼50% in solution under these conditions and that ΔG_{298} for **19** → 2 × **19_mono** is only ∼10 kJ mol^{-1}. The solution IR spectrum of **19** (like **21** and **24**) showed ν(CO) bands consistent with both bridging and nonbridging environments.

Table 1. Diffusion NMR Data for $[Co(CO)_3(PCy_3)]_2$ (15), $[Mg\{Co(CO)_3(PCy_3)\}_2(THF)]_2$ (19), $[Sr\{Co(CO)_3(PCy_3)\}_2(THF)_3]_\infty$ (21), and $[Yb\{Co(CO)_3(PCy_3)\}_2(THF)_3]_2$ (24)

compd	X-ray vol (Å^3)[a]	NMR vol (Å^3)[b]	D (mean) × 10^{-10} (m^2 s^{-1})[c]	D (Tol) × 10^{-10} (m^2 s^{-1})[c]
15	749	869	6.58	23.41
19	1788	1178	5.95	23.16
21	2269	2008	4.98	23.73
24	2296	2072	4.93	22.90

[a]Molecular volume based on the caption formula and X-ray crystal structures (estimated for a dimeric unit $[Sr\{Co(CO)_3(PCy_3)\}_2(THF)_3]_2$ for **21**) measured using 1.4 Å probe radius. [b]Molecular volume measured by diffusion NMR spectroscopy in toluene-d_8. [c]Diffusion coefficient of the compound and the residual protiosolvent in the sample under consideration (for comparison the diffusion coefficient for the protiosolvent in pure toluene-d_8 was 23.54 × 10^{-10} m^2 s^{-1}). See the SI for further details.

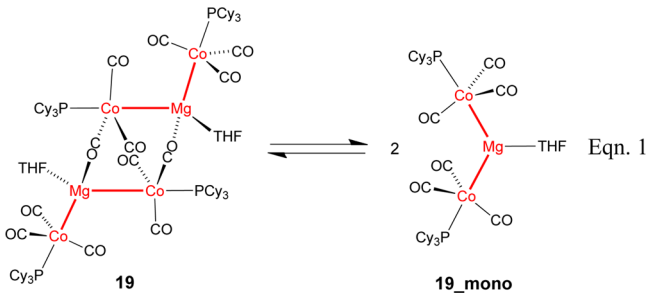

Eqn. 1

Compound **21**, although polymeric in the solid state, was determined as having an effective molecular volume of 2008 Å^3 in toluene-d_8. This is close to the value of 2296 Å^3 estimated for a dimeric moiety $[Sr\{Co(CO)_3(PCy_3)\}_2(THF)_3]_2$ based on the crystal structure. On the basis of the solution NMR and IR data alone, it is not known to what extent Sr−Co bonding is present in this dimeric species. This aspect is interrogated later on by DFT.

Beryllium and Barium. *CAUTION*: Beryllium and its compounds are highly toxic. Formation of a target compound of the type $Be\{Co(CO)_3(PCy_3)\}_2$ by reduction of $[Co(CO)_3(PCy_3)]_2$ (**15**) as successfully applied above is not possible because elemental Be does not dissolve in liquid ammonia or form an amalgam with Hg. The bulk metal is unreactive, and we avoided finely divided Be because of its extreme toxicity. Reaction of $BeCl_2$ with 1 or 2 equiv $K[Co(CO)_3(PCy_3)](THF)_2$ (**22**) in THF gave a mixture of products according to ^{31}P NMR spectroscopy, including **15**. Attempts to isolate a pure compound were unsuccessful, resulting in formation of additional **15**, even at low temperatures. Further experimental studies we not undertaken, but DFT calculations and other analyses were performed as discussed later on.

Reduction of **15** with Ba/Hg amalgam in THF under the same conditions as used for **19**−**21** afforded $Ba\{Co(CO)_3(PCy_3)\}_2(THF)_6$ (**23**) as an off-white solid in 53% isolated yield after drying in vacuo. Compound **23** is insoluble in nondonor solvents, despite the use of the lipophilic PCy_3 ligands, and crystallized from THF as a monomeric, eight-coordinate complex of the same stoichiometry as the bulk material. It has a face-capped trigonal prismatic geometry at Ba with two isocarbonyl-bonded $Co(CO)_3(PCy_3)$ groups (Figure S12 of the SI) with no residual Ba−Co bonding. The sum of

DOI: 10.1021/jacs.5b07866
J. Am. Chem. Soc. 2015, 137, 12352−12368

OC−Co−P angles is 320.3(5)°, and the Ba(1)···Co(1) separation is 5.4140(1) Å.

Insights from Ln−Co Complexes (Ln = Yb^{II}, Eu^{II}, Sm^{II}, and Sm^{III}). It is well-established that the similar covalent[25,30] and ionic[31] radii of Ca^{II} and Yb^{II} (r_{cov} = 1.76(10) and 1.87(8); r_{ionic} = 1.00 and 1.02 Å, respectively), and Sr^{II} and Eu^{II}/Sm^{II} (r_{cov} = 1.95(10) and 1.98(6) for both; r_{ionic} = 1.18 and 1.17/1.22 Å, respectively) often leads to very similar structural chemistry. We have very recently presented the first evidence of this from the point of view of Ae−TM and Ln−TM bonding through the isostructural pair of complexes $[MFp_2(THF)_3]_2$ (M = Ca (**5**) or Yb (**6**)). In these systems, the Ca−Fe bonding was found to be slightly weaker than Yb−Fe, as judged by DFT analysis and also a shorter experimental Yb−Fe bond (2.9892(4) Å) than Ca−Fe (3.0185(6) Å),[13] despite Yb having the larger radius. Likewise, the compounds $[M(^{Dipp}NacNac)(\mu\text{-}Fp)(THF)]_2$ (M = Ca or Yb) have extremely similar structures.[11b] We therefore extended our synthetic and structural studies to these selected lanthanides so as to gain further insight into structural relationships between Ae−TM and Ln−TM bonding.

Ytterbium. Reduction of **15** in THF with an excess of Yb/Hg amalgam afforded $[Yb\{Co(CO)_3(PCy_3)\}_2(THF)_3]_2$ (**24**) as a yellow solid in 62% isolated yield. Crystallization from pentane gave diffraction-quality crystals. The solid state structure shown in Figure 8 represents the first structurally authenticated example of an Ln−Co bond.

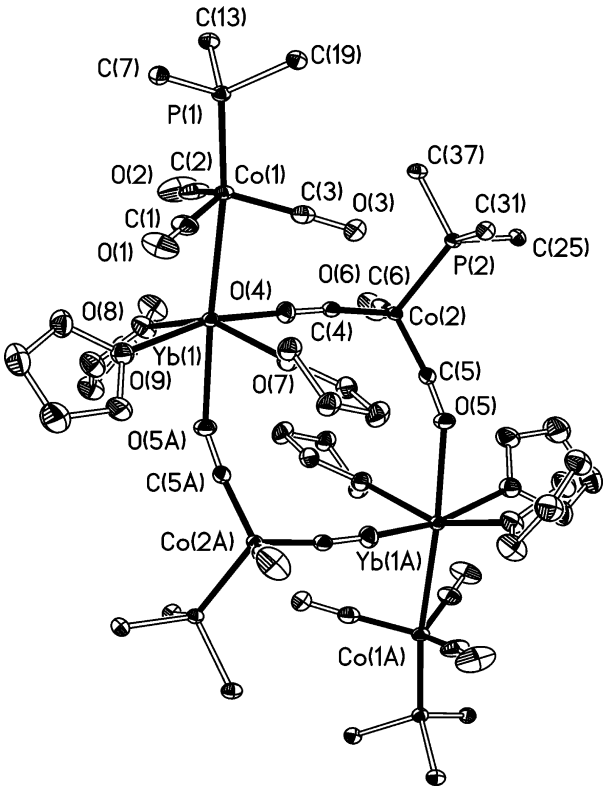

Figure 8. Displacement ellipsoid plot of $[Yb\{Co(CO)_3(PCy_3)\}_2(THF)_3]_2$ (**24**). H atoms and cyclohexyl methylene carbon atoms omitted. Distances (Å) and angles (°): Yb(1)−Co(1), 2.9893(4); Yb(1)−O(4), 2.3885(18); Yb(1)−O(5A), 2.5005(17); Yb(1)−O(7), 2.3912(17); Yb(1)−O(8), 2.4128(17); Yb(1)−O(9), 2.4258(18); C(4)−Co(2)−C(5), 105.68(11); sum of OC−Co(1)−P(1), 309.0(3); sum of OC−Co(2)−P(2), 325.5(4).

In the solid state, compound **24** exists as a discrete dimer based on two $Yb\{Co(CO)_3(PCy_3)\}_2(THF)_3$ units linked via Yb(μ-OC)Co linkages to form a central 12-membered ring. Each Yb atom forms a Yb−Co bond to a cobalt anion (Co(1)) external to this 12-membered ring and two Yb(μ-OC)Co linkages to anions within it (Co(2, 2A)). The coordination sphere is completed by three THF ligands. The Yb(1)−Co(1) bond length of 2.9893(4) Å is less than the sum of the covalent radii (3.13 Å) and is also 0.056(1) Å shorter than the Ca−Co bond in $[Ca\{Co(CO)_3(PCy_3)\}_2(THF)_2]_\infty$ (**20**, Ca(1)−Co(1) 3.0450(9) Å), despite Yb having the larger radius. As mentioned, an apparently similar observation (Δ_{M-Fe} = 0.029(1) Å) was made for the isostructural pair $[MFp_2(THF)_3]_2$ (M = Ca (**5**) or Yb (**6**)) and attributed to stronger M−Ca bonding in the case of Yb.[13] In the case of **24** and **20**, the position is not so unambiguous because in **24**, the Yb−Co bond is to an anion external to the 12-membered ring and not engaged in any further interactions, whereas for **20**, the Ca−Co bond is to an anion within an eight-membered ring, which in turn is bonded through an isocarbonyl linkage to another metal. Comparison of the "internal" and "external" (with respect to the eight-membered rings) Mg−TM bonds in $[MgFp_2(THF)]_2$ (**9**) and $[Mg\{Co(CO)_3(PCy_3)\}_2(THF)]_2$ (**19**) shows that they can differ by ∼0.06 Å on this basis alone. The sum of the OC−Co(1)−P(1) angles in **24** for the Co involved in Yb−Co bonding is 309.0(3)°. This is larger than for the external $Co(CO)_3(PCy_3)$ group in **19** (303.2(2)°), which could imply a stronger M−Co interaction in the latter case, in agreement with DFT calculations for $[CaFp_2(THF)_3]_2$ (**5**) and $[YbFp_2(THF)_3]_2$ (**6**).

Diffusion NMR analysis of **24** in toluene-d_8 (Table 1) found the effective molecular volume to be 2072 Å^3. This is close to the value estimated from the crystal structure (2296 Å^3), showing that a dimeric structure is maintained; it is also very similar to that (2008 Å^3) found for $[Sr\{Co(CO)_3(PCy_3)\}_2(THF)_3]_\infty$ (**21**), which has the same M/Co/THF ratio. These observations therefore suggest that polymeric $[Ca\{Co(CO)_3(PCy_3)\}_2(THF)_2]_\infty$ (**20**), for which diffusion NMR data could not be obtained owing to its lower solubility, might also adopt a dimeric structure in solution, although it possesses one fewer THF ligand per metal center.

Europium and Samarium. To make a comparison between $[Sr\{Co(CO)_3(PCy_3)\}_2(THF)_2\}_3]_\infty$ (**21**) and its Ln(II) analogues with similar-sized metals, the reactions of **15** with an excess of Eu/Hg or Sm/Hg amalgam were carried out. In each case, a material of overall composition "$Ln\{Co(CO)_3(PCy_3)\}_2(THF)_3$" was obtained (Ln = Eu, 75% yield, light silver-green; Ln = Sm, 83%, dark green). The behavior of these materials in THF and nondonor solvents differed significantly; we discuss the europium complex first. Diffraction-quality crystals were grown from pentane and were found to be $[Eu\{Co(CO)_3(PCy_3)_2(THF)_2\}_2]_\infty$ (**25**), isomorphous with **21**, and judged by near-identical unit cell dimensions, volume, and space group. Views of the asymmetric unit and the extended polymer chain in the solid state are shown in Figure 9.

Compound **25** retains all of the key features of its strontium counterpart: alternating 12-membered and "stretched" eight-membered rings along the one-dimensional chain, and the unique (in Ln-carbonylate anion chemistry) side-on, η^2-bound CO ligand of Co(1). Closer comparison of the two structures appears to show overall marginally shorter Sr−O distances than Eu−O ones to the same types of ligands; for example, average Sr−O_{THF} (2.550(1) Å) vs Eu−O_{THF} (2.558(2) Å) and Ln(1)−

DOI: 10.1021/jacs.5b07866
J. Am. Chem. Soc. 2015, 137, 12352−12368

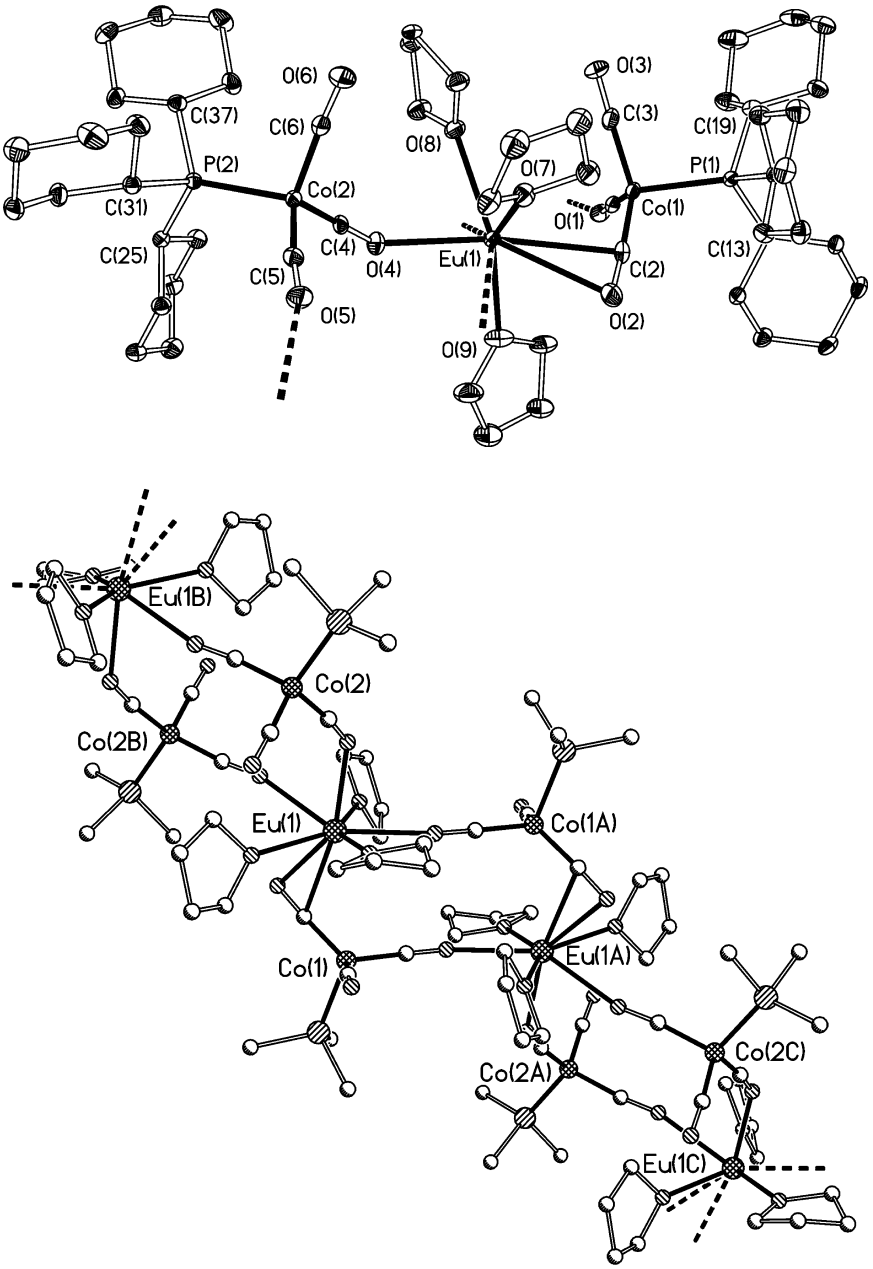

Figure 9. Displacement ellipsoid plot of the asymmetric unit (top) and ball and stick plot (bottom) of a portion of the infinite chain of $[Eu\{Co(CO)_3(PCy_3)\}_2(THF)_3]_\infty$ (**25**). H atoms and cyclohexyl methylene carbon atoms omitted. Selected distances (Å) and angles (°): Eu(1)···Co(1), 3.5551(5); Eu(1)−C(2), 2.885(3); Eu(1)−O(2), 2.916(3); Eu(1)−O(4), 2.583(3); Eu(1)−O(7), 2.544(3); Eu(1)−O(8), 2.553(2); Eu(1)−O(9), 2.576(3); sum of OC−Co(1)−P(1), 310.3(2); sum of OC−Co(2)−P(2), 326.8(2).

(μ-OC)Co(2) (Ln = Sr, 2.5639(18) vs Ln = Eu, 2.583(3) Å). In contrast, the Eu(1)···Co(1) distance of 3.5551(5) Å is significantly shorter (Å) than Sr(1)···Co(1) 3.6263(4) Å (Δ_{M-Co} = 0.071(1)). Although the Eu−Co distance is still longer than the sum of the covalent radii (3.24 Å), the shortening of the M−Co distance for M = Eu compared with M = Sr is very reminiscent of $[MFp_2(THF)_3]_2$ (M = Ca (**5**) or Yb (**6**), vide supra), which showed shorter M−Fe bonds in the case of the lanthanide, despite its larger radius and longer M−O distances).

Crystallization of **25** from THF gave $[Eu\{Co(CO)_3(PCy_3)_2(THF)_4\}_2]_\infty$, (**25·THF**) with an additional THF coordinated to each eight-coordinate Eu center (Figure S13 of the SI). This displaces the η^2-carbonyl interactions in **25** to give only Eu(μ-OC)Co linkages between metal centers and a repeating 12-membered ring motif. When the corresponding material "$Sm\{Co(CO)_3(PCy_3)\}_2(THF)_3$" was crystallized from THF, green, diffraction-quality crystals of $Sm\{Co(CO)_3(PCy_3)\}_2(THF)_6$ (**26·3THF**) were obtained, giving the structure shown in Figure 10 (left). The Sm(II) center is also eight-coordinate, with a face-capped trigonal prismatic geometry, with six THF ligands and two Sm(μ-OC)Co isocarbonyl linkages. The geometry is very similar to that of $Ba\{Co(CO)_3(PCy_3)\}_2(THF)_6$ (**23**), with which the crystals of **26·3THF** are isomorphous. The $Ba-O_{THF}$ and $Ba-O_{(\mu\text{-OC})}$ distances are all ∼0.15 Å longer than their Sm−O counterparts, as expected from the different covalent radii for the two elements (2.15(11) vs 1.98(8) Å).

DOI: 10.1021/jacs.5b07866
J. Am. Chem. Soc. 2015, 137, 12352−12368

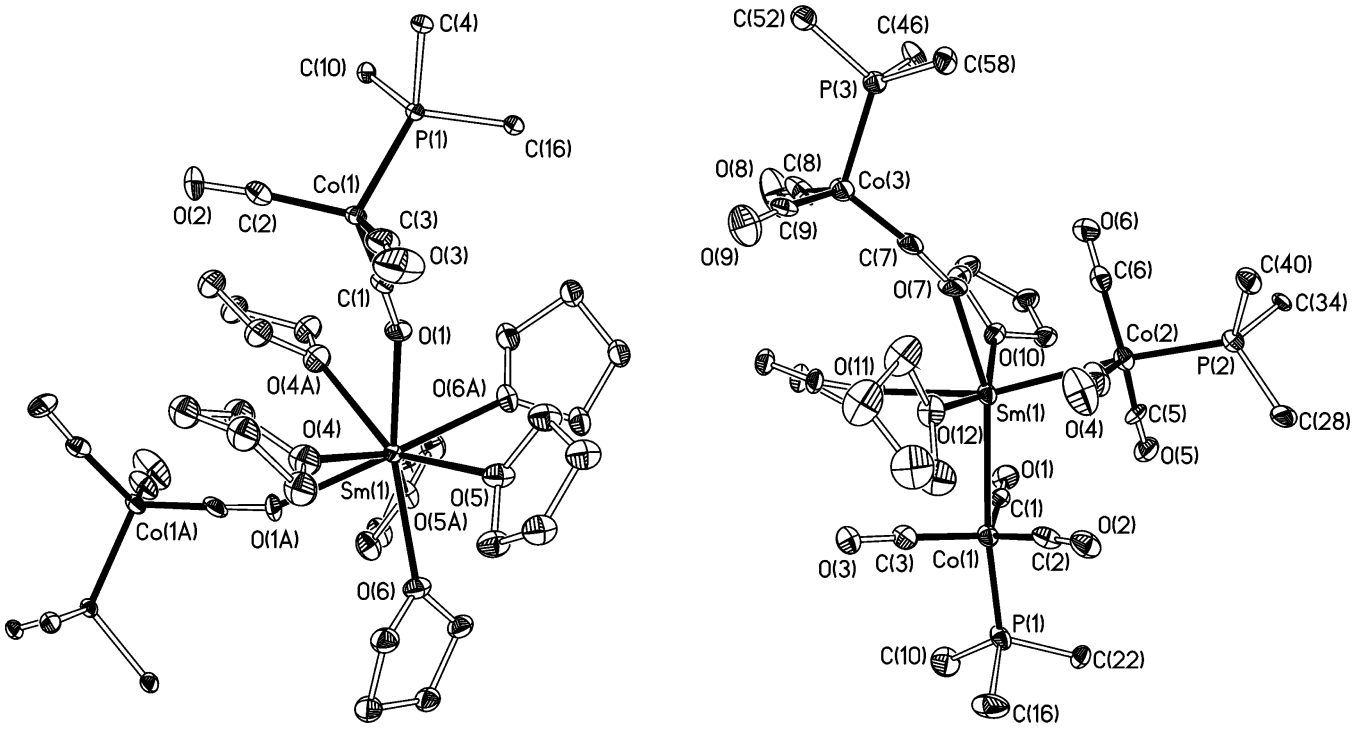

Figure 10. Displacement ellipsoid plots of $Sm\{Co(CO)_3(PCy_3)\}_2(THF)_6$ (**26·3THF**, left) and $Sm\{Co(CO)_3(PCy_3)\}_3(THF)_3$ (**27**, right). H atoms and cyclohexyl methylene carbon atoms omitted. Selected distances (Å) and angles (°) for **26·3THF**: Sm(1)−O(1), 2.543(5); Sm(1)−O(4), 2.579(7); Sm(1)−O(5), 2.702(6); Sm(1)−O(6), 2.558(5); sum of OC−Co(1)−P(1), 321.8(5). For **27**: Sm(1)−Co(1), 2.9541(10); Sm(1)−Co(2), 2.8969(9); Sm(1)−O(7), 2.346(4); Sm(1)−O(10), 2.450(4); Sm(1)−O(11), 2.452(4); Sm(1)−O(12), 2.445(4); sum of OC−Co(1)−P(1), 297.0(4); sum of OC−Co(2)−P(2), 295.8(4); sum of OC−Co(3)−P(3), 322.3(4).

Whereas $[Yb\{Co(CO)_3(PCy_3)\}_2(THF)_3]_2$ (**24**) and $[Eu\{Co(CO)_3(PCy_3)\}_2(THF)_3]_\infty$ (**25**) can be dissolved in pentane or benzene/toluene without change, dissolving **26** in either of these solvents immediately gave a color change to dark red and the formation of a gray, metallic residue. On scale-up, dissolving 450 mg of $Sm\{Co(CO)_3(PCy_3)\}_2(THF)_3$ (**26**) in benzene afforded ∼350 mg of the Sm(III) compound $Sm\{Co(CO)_3(PCy_3)\}_3(THF)_3$ (**27**, 86% yield). The X-ray structure of **27** is shown in Figure 10 (right) and confirms the formation of **27** by a spontaneous solvent-induced disproportion reaction of the Sm(II) precursor **26**. Compound **27** can also be formed in 71% isolated yield by reaction of SmI_2 with $K[Co(CO)_3(PCy_3)](THF)_2$ (**22**) in THF (initially forming **26**), followed by extraction into benzene.

The geometry at the six-coordinate Sm(1) is approximately octahedral and comprises two Sm−Co bonds (Sm(1)−Co(1) = 2.9541(10), Sm(1)−Co(2) = 2.8969(9) Å), an isocarbonyl linkage to the other $Co(CO)_3(PCy_3)$ moiety, and three THF ligands. The Sm−Co bond lengths are within the sum of the covalent radii (3.24 Å).[25] The geometries at the Sm-bonded atoms Co(1) and Co(2) are close to trigonal bipyramidal, and the sums of the OC−Co(1)−P(1) and OC−Co(2)−P(2) angles are 297.0(4)° and 295.8(4)°, consistent with significant Sm−Co interactions. The geometry at Co(3) is approximately tetrahedral, and the sum of the OC−Co(3)−P(3) angles is 322.3(4)°, similar to that for the isocarbonyl-bound anion in **26·3THF** (321.8(5)°). The average $Sm-O_{THF}$ (2.449(2) Å) and $Sm-O_{(\mu\text{-OC})}$ (2.346(4) Å) distances for **27** are considerably shorter than those for **26·3THF** (2.613(3) and 2.543(5) Å, respectively), commensurate with the change in oxidation state from Sm^{II} to Sm^{III} (ionic radii 1.27 and 0.958 Å, respectively)[31] and the decrease in coordination number. Compound **27** represents the first example of a structurally authenticated complex with a Sm−Co bond, Kempe's $Sm(Cp_2Re)_3$ representing the only other complex with a Sm−TM bond.[6e]

The stability of $[Yb\{Co(CO)_3(PCy_3)\}_2(THF)_3]_2$ (**24**) and $[Eu\{Co(CO)_3(PCy_3)\}_2(THF)_3]_\infty$ (**25**) toward the same type of disproportionation is attributed to the higher stability of the $4f^7$ and $4f^{14}$ configurations of Eu(II) and Yb(II) compared with the $4f^6$ one of Sm(II).[32] The driving force for the solvent-dependent disproportionation in the case of **26** is unclear, but we note in this context that Evans et al. reported the reaction of $[Co(CO)_4]_2$ with $Cp^*_2Sm(THF)_2$ to form the Sm(III) species $Cp^*_2Sm\{Co(CO)_4\}(THF)$ (without structural characterization). Similarly, reaction of $[Co(CO)_4]_2$ with $SmI_2(THF)_x$ in THF gave the Sm(III)/Co(-I) ion pair $[SmI_2(THF)_5][Co(CO)_4]$.[33]

Computational Studies of Ae−Co Complexes. Detailed computational studies and reviews of polar metal−metal bonds involving either f-element−TM[6a,f,8b,c,g,13,34] or TM−TM (early late heterobimetallic systems)[15,23a] have been described. Within the context of Ae−metal bonding, most computational studies have focused on $(L)Ae^I-Ae^I(L)$ systems.[3a] The general periodic trends within group 2 are well-established.[32,35] We have reported briefly on the Ca−Fe bonding in $[CaFp_2(THF)_3]_2$ (**5**) and its ytterbium analogue, **6**.[13] The bonding was similar in each case (predominantly electrostatic), but the Yb−Fe interactions were found to be slightly stronger than for Ca−Fe.

To gain a more comprehensive understanding of the structures and bonding of the new Ae−Co complexes described above, we carried out detailed computational studies on a series of model and hypothetical complexes. We used a combination of gradient-corrected density functional theory (DFT)

DOI: 10.1021/jacs.5b07866
J. Am. Chem. Soc. 2015, 137, 12352−12368

Table 2. Selected Computational Results for $[Mg\{Co(CO)_3(PMe_3)\}_2(THF)]_2$ (19Q), $Mg\{Co(CO)_3(PMe_3)\}_2(THF)$ (19_monoQ) and $[Mg\{Co(CO)_4)\}_2(THF)]_2$ (28Q), $[Be\{Co(CO)_3(PMe_3)\}_2]_2$ (29Q), $Be\{Co(CO)_3(PMe_3)\}_2(THF)$ (30Q), $[Ca\{Co(CO)_3(PMe_3)\}_2(THF)_2]_2$ (20Q), $[Ca\{Co(CO)_3(PMe_3)\}_2(THF)_3]_2$ (20·THFQ), $[Sr\{Co(CO)_3(PMe_3)\}_2(THF)_3]_2$ (21Q), and $[Sr\{Co(CO)_3(PMe_3)\}_2(THF)_4]_2$ (21·THFQ)[a]

	19Q	19_monoQ	28Q	29Q	30Q	20Q	20·THFQ	21Q	21·THFQ
Ae−Co(1) (Å)[b]	2.598	2.486	2.655	2.206	2.182	2.996	3.031	3.249	3.399
Ae−Co(2) (Å)[b]	2.528	2.480	2.547	2.154	2.183	3.168	4.753	3.204	4.880
∑(OC−Co(1)−L) (deg)[b]	295.9	298.9	303.1	297.8	297.2	297.1	298.7	303.3	281.7
∑(OC−Co(2)−L) (deg)[b]	301.1	298.0	307.4	296.1	297.3	314.6	323.1	301.7	321.6
Q Ae	0.79	0.66	0.80	0.48	0.57	1.25	1.35	1.30	1.45
Q Co(1)	−0.32	−0.35	−0.20	−0.28	−0.37	−0.26	−0.24	−0.24	−0.24
ΔQ |Ae-Co(1)|	1.11	1.01	1.00	0.76	0.94	1.51	1.59	1.54	1.69
Q Co(2)	−0.35	−0.35	−0.24	−0.38	−0.37	−0.28	−0.16	−0.30	−0.24
ρ,[c] Ae−Co(1)	0.026	0.032	0.025	0.049	0.051	0.021	0.019	0.016	0.013
ρ,[c] Ae−Co(2)	0.030	0.032	0.030	0.054	0.051	*f*	*f*	0.016	*f*
$\nabla^2\rho$,[d] Ae−Co(1)	0.060	0.077	0.053	0.011	0.013	0.038	0.038	0.039	0.034
$\nabla^2\rho$,[d] Ae−Co(2)	0.072	0.077	0.068	0.014	0.013	*f*	*f*	0.042	*f*
H,[c] Ae−Co(1)	−0.003	−0.005	−0.003	−0.025	−0.026	−0.002	−0.001	−0.0002	0.0005
H,[c] Ae−Co(2)	−0.004	−0.005	−0.004	−0.028	−0.026	*f*	*f*	−0.0004	*f*
interaction energy[e]	−216.9		−192.5	−242.3		−163.2	−147.3	−137.9	−129.9
orbital mixing energy[e]	−201.7		−167.0	−356.2		−104.4	−91.9	−85.3	−99.6
electrostatic interaction energy[e]	−256.7		−211.9	−310.0		−193.2	−175.4	−171.5	−153.9
Pauli repulsion energy[e]	241.5		186.4	419.1		134.4	119.9	118.9	108.4

[a]Interaction energies refer to combining the individual $Ae\{Co(CO)_3(L)\}_2(THF)_n$ fragments in the dimeric compounds and by definition are not given for **19_monoQ** and **30Q**. [b]L = PMe_3 or CO_{ax}, for dimeric structures; Co(1) and Co(2) refer to the atoms within or external to the eight-membered ring, respectively. [c]Electron density. [d]Electron density Laplacian. [e]Per Ae−Co bond in kJ mol^{-1} (orbital mixing (and hence, total interaction) energies corrected for basis set superposition error (**29Q**, 4.8; **19Q**, 6.7; **28Q**, 6.7; **20Q**, 6.3; **20·THFQ**, 5.8; **21Q**, 6.6; **21·THFQ**, 7.6). [f]No Ae−Co(2) bond path. BCP data are given in atomic units; charges *Q* are from Mulliken analyses.

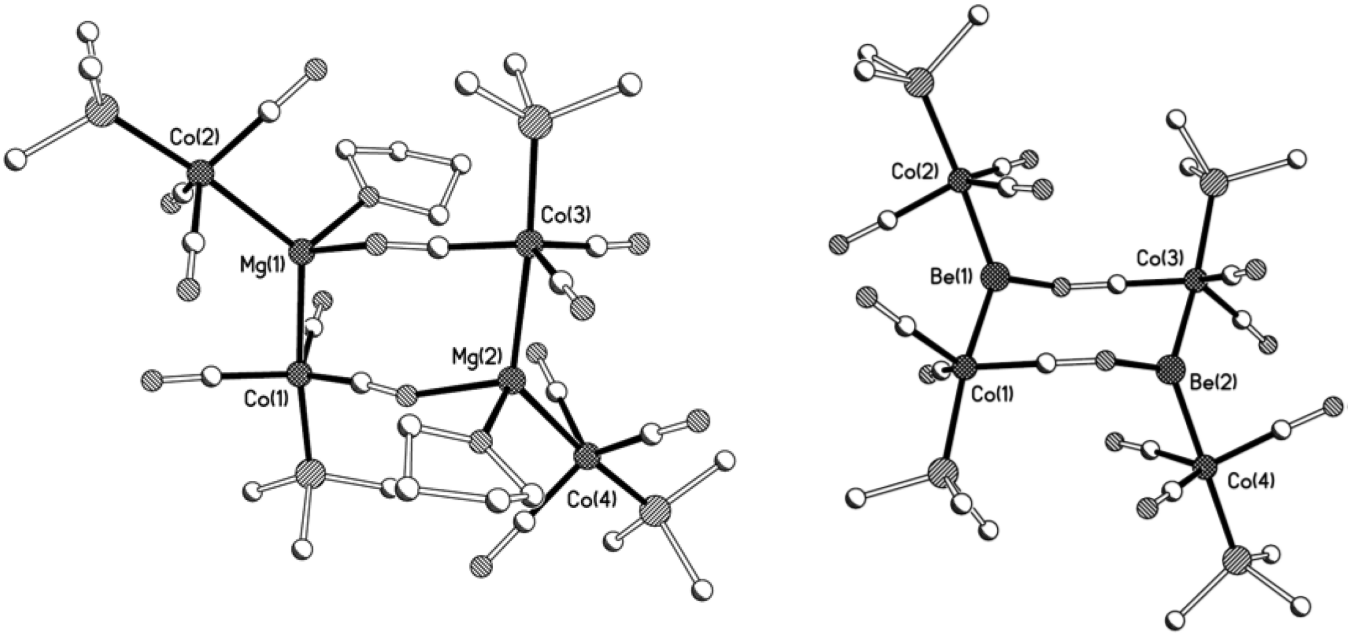

Figure 11. DFT structures of $[Mg\{Co(CO)_3(PMe_3)\}_2(THF)]_2$ (**19Q**, left) and $[Be\{Co(CO)_3(PMe_3)\}_2]_2$ (**29Q**, right). See the text and Table 2 for further details.

calculations (without symmetry constraints) for geometry optimization, the Ziegler Rauk energy decomposition analysis (EDA) scheme,[36] and atoms in molecules (AIM)[37] analysis. We focus primarily on the experimentally well-defined magnesium, calcium, and strontium systems **19**−**21** but with the PCy_3 substituent of $Co(CO)_3(PCy_3)$ replaced by the more computationally feasible PMe_3 (the electronic differences are not significant in this context[38]). We also included in these studies three beryllium systems that we were unable to access experimentally. Barium complexes were not studied and are expected to continue the trends established below for Be to Sr, which are clearly implied by experiment for **18** and **23**. The key results of the calculations are summarized in Table 2. Compound numbers for the computed complexes are distinguished from their experimental counterparts by the suffix **Q**.

DOI: 10.1021/jacs.5b07866
J. Am. Chem. Soc. 2015, 137, 12352−12368

Beryllium and Magnesium. As a starting point, $[Mg\{Co(CO)_3(PMe_3)\}_2(THF)]_2$ (**19Q**) was optimized as a model for the crystallographically characterized dimer, $[Mg\{Co(CO)_3(PCy_3)\}_2(THF)]_2$ (**19**). The DFT structure of **19Q** (Figure 11) reproduces very well the main features of the real complex (Figure 4). In particular, the Mg−Co distances internal to the ring (calcd, 2.598; X-ray, 2.6163(6) Å) are ∼0.07 Å longer than those external to it (calcd, 2.528; X-ray,: 2.5427(6) Å), features that were also found in $[MgFp_2(THF)]_2$ (**9**). The sums of the OC−Co−P angles are similar, with the values subtended at Co(1) being slightly smaller than those at Co(2) in both the DFT and X-ray structures.

Table 2 summarizes selected AIM data at the Ae−TM bond critical points (BCPs) and Mulliken charge (Q) data for Ae and Co. The AIM data support the presence of Mg−Co bonds by finding the expected bond paths. The large ΔQ values (difference in Mulliken atomic charges for Ae and Co), the small positive values of both ρ (electron density) and its Laplacian $\nabla^2\rho$, and the small negative H values confirm the Ziegler−Rauk analyses (see below) and our previous studies of **5** in finding little covalency in the bonding that has mainly ionic character. We note that the BCP data indicate "metallic bonding" in the Bianchi approach.[39] The values of ρ and $\nabla^2\rho$ are comparable for the Mg−Co bonds internal to and external to the eight-membered ring, although the ones for Mg(1)−Co(2 (external)) are slightly larger, as would be expected from the shorter bond length.

Ziegler−Rauk energy decomposition analysis[36] was used to assess the interaction between two $Mg\{Co(CO)_3(PCy_3)\}\{(\mu\text{-}OC)Co(CO)_2(PCy_3)\}(THF)$ fragments of **19Q** (frozen at the converged geometry) upon forming the Mg(1)−Co(1) and Mg(2)−Co(3) bonds of the central eight-membered ring. This approach was chosen because it allows the best comparison of the Ae−Co interactions among all the various dimeric $Ae\{Co(CO)_3(PCy_3)\}_2(THF)_n$ (n = 0−4) complexes (Ae = Be − Sr). Although the geometry and coordination number around Ae changes for these compounds, as does the type of bonding to the external cobalt group (i.e., direct Ae−Co or isocarbonyl bridge), all of the model and experimental systems form some variation of an eight-membered ring with some degree of internal Ae−Co interaction. The EDA data for **19Q** found a significant interaction energy between the two fragments of −216.9 kJ mol^{-1} per bond. The relative contributions of the prerelaxation electrostatic term and the postrelaxation orbital mixing term support the AIM data and Mulliken atomic charges in implying that the Mg−Co bonds are predominantly ionic. The favorable orbital mixing contributions to the Mg−Co interaction energy do not indicate significant covalency and, in fact, represent redistribution of charge within each fragment on relaxation to self-consistency.[13]

Experimentally (Table 1, eq 1), the solution diffusion NMR data implied that **19** partially dissociates in solution, feasibly to the monomeric species $Mg\{Co(CO)_3(PCy_3)\}_2(THF)$ (**19_mono**). A model of this was computed: **19_monoQ**. The key data are given in Table 2, and the structure is shown in Figure S14 of the SI. The geometry at Mg is approximately trigonal planar with shorter Mg−Co distances (Δ_{Mg-Co} = ∼0.08 Å (av)) than in **19Q** and slightly larger values of both ρ and $\nabla^2\rho$, as would be expected from the lower coordination number. The computed ΔG_{298} for **19Q** → 2 **19_monoQ** is 22.0 kJ mol^{-1}, which is comparable with the value estimated experimentally by diffusion NMR measurements (∼10 kJ mol^{-1}). The smaller experimental value could reflect various factors, not the least of which is the larger steric crowding in the real system **19**.

As mentioned, the donor ability of $[Co(CO)_3(L)]^-$ both to other transition metals in early late heterobimetallics and to hydrogen bond donors R_3NH^+ can be improved by using a more strongly σ-donating L = phosphine in place of L = CO. Experimentally, we found that reduction of $[Co(CO)_3(L)]_2$ (L = CO or PPh_3) with Ae/Hg amalgam gave insoluble materials that were either intractable or could be crystallized only from THF, disrupting any possible Ae−Co interactions. To gain further insight into the possible influence of the cobalt substituent L in the structure and bonding in these molecules, the Co-bound PMe_3 group in **19Q** was substituted by CO to give $[Mg\{Co(CO)_4\}_2(THF)]_2$ (**28Q**). Key data are given in Table 2 and a view of the molecule is shown in Figure S15 of the SI. In addition, we also calculated the electronic structure of the free cobalt anions $[Co(CO)_3(L)]^-$, frozen in the geometry of the optimized corresponding hydride Co(H) $(CO)_3(L)$ prior to removal of H^+. The isosurfaces of the HOMOs (metal-based, mainly d_z^2 in character) are shown in Figure S16 of the SI. The most important point to note is that the HOMO in $[Co(CO)_3(PCy_3)]^-$ is 0.39 eV less stablilized than in $[Co(CO)_4]^-$, which is consistent with the observed increased nucleophilicity of the former as judged by previous experimental systems.[23b]

The overall geometry and main structural features for **19Q** are conserved in **28Q**; however, the EDA shows a significantly reduced Mg−Co interaction energy between the $Mg\{Co(CO)_4\}_2(THF)$ fragments in **28** (−192.5 vs −216.9 kJ mol^{-1} per metal−metal bond). This is accompanied by lengthened Mg−Co bonds both within and external to the eight-membered ring, although the AIM parameters at the BCPs change relatively little.

As described below, the decrease in Ae−Co EDA interaction energy on changing from Ca−Co to Sr−Co bonding in the model complexes $[Ca\{Co(CO)_3(PMe_3)\}_2(THF)_2]_2$ (**20Q**) and $[Sr\{Co(CO)_3(PMe_3)\}_2(THF)_3]_2$ (**21Q**) is ∼25 kJ mol^{-1} per Ae−Co bond. This is the same as the change for Mg−Co on changing from $Co(CO)_3(PCy_3)$ to $Co(CO)_4$ (∼24 kJ mol^{-1} per bond). Although we have not been able to test this computational result experimentally, it certainly strongly suggests that there is both a substantial electronic as well as a solubility advantage (i.e., for avoiding THF or another donor solvent) in using the PCy_3-substituted carbonylate anion in studies of M—Co bond chemistry.

Although our experimental efforts to prepare a compound with a Be−Co bond were unsuccessful, we were nonetheless interested in evaluating the electronic properties of some models of the target systems for comparison with their heavier Ae−Co congeners. We have found experimentally (in the absence of an excess of competing THF or other Lewis bases) that Ae−Co bonding is favored by an increasing charge/size ratio of the Ae or Ln center. In addition, calculations on (L)Ae−Ae(L) dimers find the largest BDEs for Ae = Be (e.g.[40] for L = Ph, Ae = Be, Mg or Ca, BDE = 286, 167, 89 kJ mol^{-1}). We have evaluated three model compounds: two-coordinate $Be\{Co(CO)_3(PMe_3)\}_2$ (**31Q**, Figure S17 of the SI); its THF adduct $Be\{Co(CO)_3(PMe_3)\}_2(THF)$ (**30Q**, Figure S17) analogous to **19_monoQ**; and the dimer of **31Q**, $[Be\{Co(CO)_3(PMe_3)\}_2]_2$ (**29Q**, Figure 11), so as to allow a comparison of EDA data with the dimeric compounds for Ae = Mg − Sr. Key data for **30Q** and **29Q** are listed in Table 2, and those for **31Q** are given in Table S1 of the SI. ΔG_{298} for

DOI: 10.1021/jacs.5b07866
J. Am. Chem. Soc. 2015, 137, 12352−12368

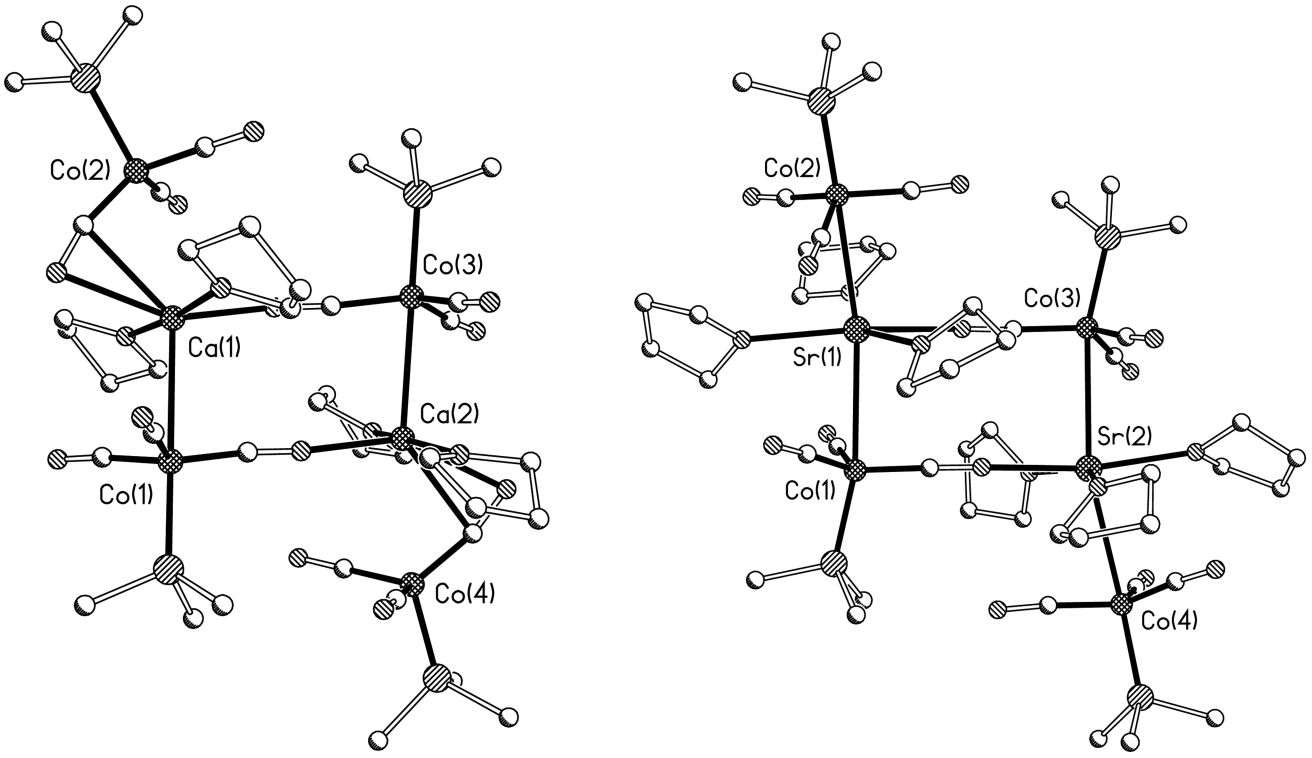

Figure 12. DFT structures of $[Ca\{Co(CO)_3(PMe_3)\}_2(THF)_2]_2$ (**20Q**, left) and $[Sr\{Co(CO)_3(PMe_3)\}_2(THF)_3]_2$ (**21Q**, right). See the text and Table 2 for further details.

31Q + THF → **30Q** was only 0.8 kJ mol^{-1}; in contrast, ΔG_{298} for the dimerization reaction 2 × **31Q** → **29Q** was 50.2 kJ mol^{-1}. Therefore, real systems of the type "$Be\{Co(CO)_3(PR_3)\}_2$" should exist either as a two-coordinate monomer or a weakly coordinated Lewis base adduct.

For the purpose of comparison with the other complexes, we focus just on $[Be\{Co(CO)_3(PMe_3)\}_2]_2$ (**29Q**) and $Be\{Co(CO)_3(PMe_3)\}_2(THF)$ (**30Q**). As expected from the smaller covalent radius for beryllium (r_{cov} = 0.96(3) (Be) vs 1.41(7) (Mg)), compound **29Q** (Figure 11) has shorter Be−Co distances both internal to the eight-membered ring and external to it (this being the shorter of the two, as expected). The interaction energy between the $Be\{Co(CO)_3(PMe_3)\}_2$ fragments (−242.3 kJ mol^{-1} per bond) is 25.4 kJ mol^{-1} more favorable than for **19Q**. The significantly larger values of ρ, $\nabla^2\rho$, and H and the smaller ΔQ |Ae−Co(1,2)| values point toward a less ionic bonding position, consistent with expectations. These trends are mirrored in the corresponding data for the THF adducts, **30Q** and **19_monoQ**. Small decreases in the $\sum$(OC−Co(1,2)−PCy_3) angles are also observed in the beryllium complexes compared with their magnesium counterparts.

We noted previously[13] that it is highly unusual for the electrostatic EDA term to be the largest (in an absolute sense) for systems with neutral fragments. This is also true here (Table 2) for the Mg (**19Q**), Ca (**20Q**), and Sr (**21Q**) systems, but not for the Be congener (**29Q**), for which it is the smallest in absolute terms. This is consistent with larger covalent interactions in the Be systems.

Calcium and Strontium. Experimentally, calcium forms a toluene-soluble complex **20** of stoichiometry "$Ca\{Co(CO)_3(PCy_3)\}_2(THF)_2$" and crystallizes as $[Ca\{Co(CO)_3(PCy_3)\}_2(THF)_2]_\infty$ (Figure 6) in the solid state. In contrast to the dimeric yttrium analogues $[Yb\{Co(CO)_3(PCy_3)\}_2(THF)_3]_2$ (**24**) and $[CaFp_2(THF)_3]$ (**5**), which have three THF ligands per Ae or Ln, **20** necessarily forms a polymeric (isocarbonyl bridged) structure to achieve six-coordination. Similarly, **21** forms "$Sr\{Co(CO)_3(PCy_3)\}_2(THF)_3$" according to ^{1}H NMR and elemental analysis and achieves seven-coordination through chain formation in the solid state. Diffusion NMR spectroscopy established that both **21** and **24** maintain a dimeric structure in solution. It is entirely reasonable to assume that **20** will maintain a predominantly dimeric structure in solution (cf. $[Mg\{Co(CO)_3(PCy_3)\}_2(THF)]_2$ (**19**), which also favors a dimeric form).

DFT geometry optimizations were first carried out on model dimers with the experimental stoichiometry (i.e. $[Ca\{Co(CO)_3(PMe_3)\}_2(THF)_2]_2$ (**20Q**) and $[Sr\{Co(CO)_3(PMe_3)\}_2(THF)_3]_2$ (**21Q**)) starting from geometries based on the eight-membered units of the experimental X-ray structures with one isocarbonyl bridging group from a neighboring moiety removed. These results are shown in Figure 12.

$[Ca\{Co(CO)_3(PMe_3)\}_2(THF)_2]_2$ (**20Q**) possesses the now-familiar eight-membered ring with an internal Ca(1)−Co(1) bond slightly shorter than in the experimental system (2.996 vs 3.0450(9) Å). The two THF ligands are mutually trans, and the remaining $Co(CO)_3(PMe_3)$ binds in an η^2 (side-on) manner reminiscent of that in $[Sr\{Co(CO)_3(PCy_3)\}_2(THF)_3]_\infty$ (**21**, Figure 7), apparently attempting to span the two remaining coordination sites at Ca(1). The Ca(1)···Co(2) distance of 3.168 Å is significantly larger than Ca(1)−Co(1) and exceeds the sum of the covalent radii (3.02 Å). The $\sum$(OC−Co(1)−PCy_3) value is 297.1°, which is consistent with the short Ca(1)−Co(1) distance, but the $\sum$(OC−Co(2)−PCy_3) value of 314.6° implies little Ca(1)−Co(2) bonding. Consistent with

DOI: 10.1021/jacs.5b07866
J. Am. Chem. Soc. 2015, 137, 12352−12368

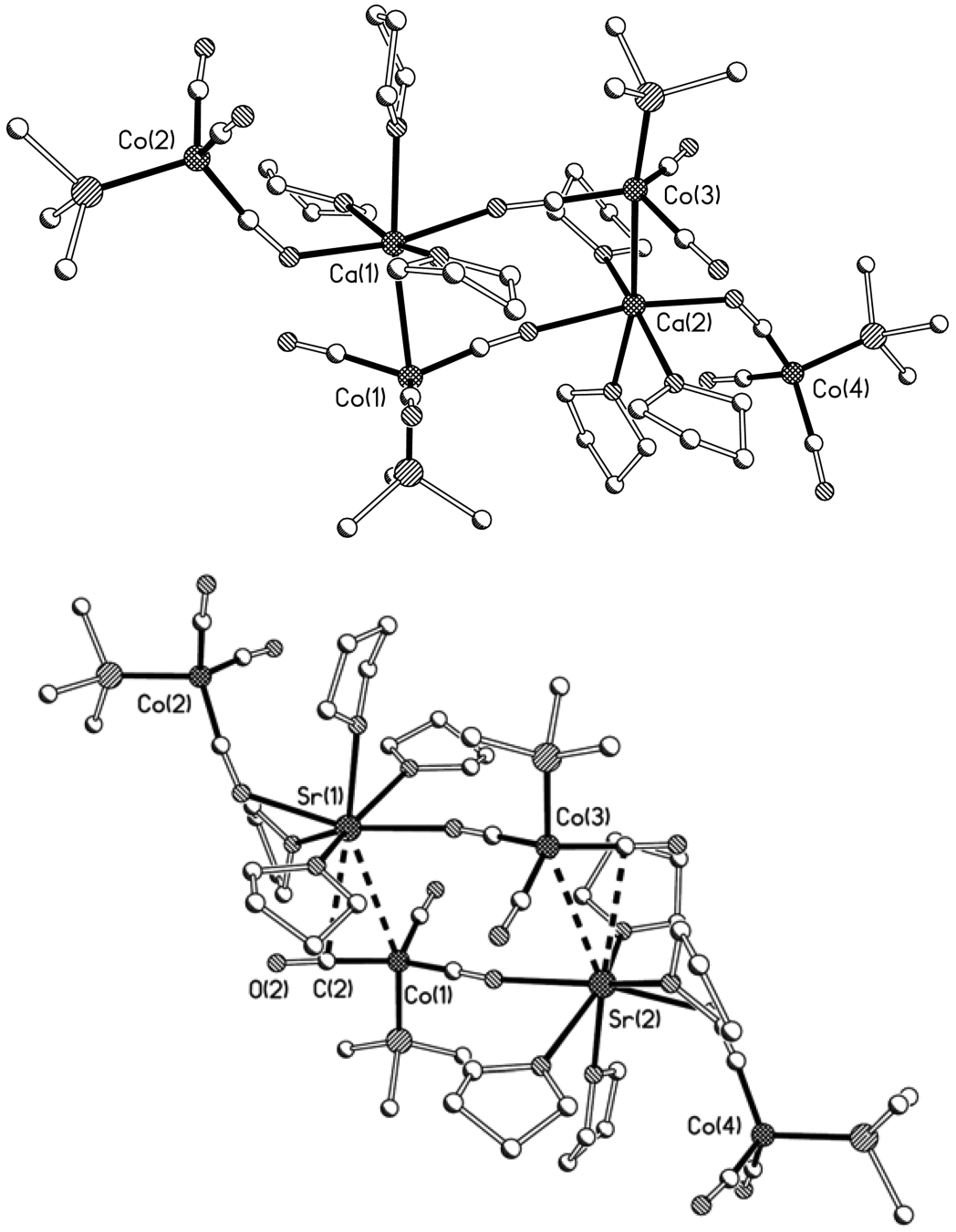

Figure 13. DFT structures of $[Ca\{Co(CO)_3(PMe_3)\}_2(THF)_3]_2$ (**20·THFQ**, top) and $[Sr\{Co(CO)_3(PMe_3)\}_2(THF)_4]_2$ (**21·THFQ**, bottom). See the text and Table 2 for further details.

these geometrical features, AIM analysis found no bond path between Ca(1) and Co(2).

In the absence of additional (isocarbonyl) donors from neighboring units in the polymeric chain, $[Sr\{Co(CO)_3(PMe_3)\}_2(THF)_3]_2$ (**21Q**) has a structure (Figure 12, right) quite different from the solid state one and shows many features of the experimental calcium, ytterbium, and magnesium systems. It contains six-coordinate strontium ions at the vertices of an eight-membered ring that contains Sr(1,2)−Co(1,3) bonds of ∼3.249 Å, close to the sum of the covalent radii (3.21 Å). External to this ring are two other Sr−Co bonds (∼3.204 Å) that, as expected, are slightly shorter than the internal bonds. The sums of the OC−Co(1)−PMe_3 angles subtended at Co(1) (303.3°) and Co(2) (301.7°) are typical of metal−metal bonded groups, and AIM analysis found bond paths for both Sr(1)−Co(1) and Sr(1)−Co(2).

To simulate the increase in coordination number caused by the bridging isocarbonyl groups from neighboring moieties in the polymeric chain, an additional THF ligand was added to each DFT model forming $[Ca\{Co(CO)_3(PMe_3)\}_2(THF)_3]_2$ (**20·THFQ**) and $[Sr\{Co(CO)_3(PMe_3)\}_2(THF)_4]_2$ (**21·THFQ**), which were optimized. These results are shown in Figure 13.

Addition of another THF to each Ca in **20Q** to form **20·THFQ** completely displaces the previously side-on bound CO ligand of Co(2) to give a conventional six-coordinate calcium.

DOI: 10.1021/jacs.5b07866
J. Am. Chem. Soc. 2015, 137, 12352−12368

The eight-membered ring is maintained, as in the experimental solid state structure, and the Ca(1)−Co(1) distance of 3.031 Å matches well with the observed one of 3.0450(9) Å. The geometry of this model is also very close to that found experimentally for **5**. The sums of the OC−Co−PMe_3 angles for Co(1) and Co(2) are within the ranges expected (298.7 and 323.1°, respectively).

Addition of another THF to each Sr center of **21Q** changes the structure very substantially, and it (**21·THFQ**) now quite closely matches that in the solid state. The formerly directly bonded Co(2) of **21Q** has completely rearranged to an isocarbonyl-bridged system ($\sum$(OC−Co(2)−PMe_3) = 321.6°). The eight-membered ring has become "stretched" as the Sr(1, 2)−Co(1, 3) distances have increased from ∼3.249 to ∼3.399 Å, and there is now a somewhat closer Co(1)···C(2) distance of 3.128 Å. Experimentally, the Sr(1)···Co(1) and Sr(1)−C(2) values are 3.6263(4) and 2.909(2) Å, respectively. The DFT Sr(1)−Co(1) distance of 3.399 Å is clearly at the limits of the sum of the covalent radii (3.21 Å), but the AIM analysis found a bond bath and BCP. Although **21·THFQ** differs more than the other models from the experimental system that it is trying to model, the general agreement and overall direction of travel is very good indeed for these large and rather "soft" systems.

The EDA, AIM, and Mulliken charge data for **20Q** − **21·THFQ** follow the trends established for $[Mg\{Co(CO)_3(PMe_3)\}_2(THF)]_2$ (**19Q**), $[Be\{Co(CO)_3(PMe_3)\}_2]_2$ (**29**), and their homologues. Thus, the interaction energies between $Ae\{Co(CO)_3(PMe_3)\}_2(THF)_n$ fragments decrease from **19Q** to **20Q** to **21Q** while the values of ρ, $\nabla^2\rho$, and ΔQ |Ae-Col values point toward increasingly ionic systems. The interaction energy of −147.3 kJ mol^{-1} for each Ca−Co bond in six-coordinate $[Ca\{Co(CO)_3(PMe_3)\}_2(THF)_3]_2$ (**20·THFQ**) is slightly larger than the corresponding value of 134.9 kJ mol^{-1} for each Ca−Fe bond in the otherwise analogous $[CaFp_2(THF)_3]$ (**5**), suggesting that $Co(CO)_3(PCy_3)$ is a better-suited probe of Ae−TM bonding than Fp, both on electronic grounds and in terms of superior solubility in nondonor solvents.

CONCLUSIONS AND SUMMARY

We have comprehensively established the scope, limitations, and nature of Ae−TM bonding using the $[Co(CO)_3(PCy_3)]^-$ anion as an exemplar. This is supported by new and recently communicated complementary results based on Fp^-; namely, $[MgFp_2(THF)]_2$ (**19**), $[CaFp_2(THF)_3]_2$ (**5**), and $[YbFp_2(THF)_3]_2$ (**6**). The privileged nature of $[Co(CO)_3(PCy_3)]^-$ can be traced to inherently stronger Ae−Co bonds (than, for example, with $[Co(CO)_4]^-$ or Fp^-, as judged by Ziegler−Rauk energy decomposition analysis) and, critically, the enhanced solubility of the products in nondonor hydrocarbon solvents. The "isocarbonyl problem" still remains in the solid state, even when using $[Co(CO)_3(PCy_3)]^-$, as judged by the polymeric structures for $[Ca\{Co(CO)_3(PCy_3)\}_2(THF)_2]_\infty$ (**20**) and, especially, $[M\{Co(CO)_3(PCy_3)\}_2(THF)_3]_\infty$ (M = Sr (**21**) or Eu (**25**)). However, in solution, the available experimental and DFT evidence points to Sr−Co bonding being perfectly viable in the absence of Lewis base donors, as supported by diffusion NMR measurements for selected systems.

As judged by experiment for the series $[Mg\{Co(CO)_3(PCy_3)\}_2(THF)]_2$ (**19**, two Co−Mg bonds), $[Ca\{Co(CO)_3(PCy_3)\}_2(THF)_2]_\infty$ (**20**, one Co−Ca bond), $[Sr\{Co(CO)_3(PCy_3)\}_2(THF)_3]_\infty$ (**21**, one side-on bound CO ligand a long Co···Sr distance), and $Ba\{Co(CO)_3(PCy_3)\}_2(THF)_6$ (**23**, no Co−Ba bond) Ae−TM bonding becomes weaker going down the group. The computational studies of structure and geometry, Ziegler−Rauk energy decomposition analysis, and atoms in molecules analysis for the series $[Ae\{Co(CO)_3(PMe_3)\}_2(THF)_n]_x$ (Ae = Be, Mg, Ca, Sr; n = 0−4; x = 1 or 2) also found that the Ae−Co (fragment) interaction energy decreased in this order, with that for Be−Co being approximately twice that for Sr−Co. The Ae−Co bonding also becomes increasingly ionic in this order. Toward the bottom of the Ae group, side-on (η^2) CO ligand coordination competes with direct Ae−Co bonding, especially as the coordination number of the Ae is increased by addition of further donors.

Our previous communication reported that the similarly sized Ca^{II} and Yb^{II} ions led to isomorphous structures $[CaFp_2(THF)_3]_2$ (**5**) and $[YbFp_2(THF)_3]_2$ (**6**), with slightly shorter Yb−Fe bonds than Ca−Fe, opposite to the expectations based on the metal radii. In our current work, we found that this also extends to the larger metals Sr^{II} and Eu^{II}, as judged by the solid state structures of $[M\{Co(CO)_3(PCy_3)\}_2(THF)_3]_\infty$ (M = Sr (**21**) or Eu (**25**)). Although $[Ca\{Co(CO)_3(PCy_3)\}_2(THF)_2]_\infty$ and $[Yb\{Co(CO)_3(PCy_3)\}_2(THF)_3]_2$ exist as polymeric and dimeric compounds in the solid state, the general principles of forming one M−Co bond and one M(μ-OC)Co η^1-isocarbonyl linkage to the $Co(CO)_3(PCy_3)$ moieties persist (M = Ca or Yb).

An unexpected but important result of general relevance was the disproportionation of $Sm^{II}\{Co(CO)_3(PCy_3)\}_2(THF)_3$ (**26**) to $Sm^{III}\{Co(CO)_3(PCy_3)\}_3(THF)_3$ (**27**) in nondonor solvent. This allowed for the first time, within an otherwise identical environment, the effect of charge on Ln−TM bonding to be established because it can reasonably be assumed that the Eu^{II} compound $[Eu\{Co(CO)_3(PCy_3)\}_2(THF)_3]_\infty$ (**25**) is a fair model for **26** (Sm^{II}), so the presence of two short, direct Sm−Co bonds in **27** reflects the effect of this increase in charge and concomitant decrease in radius. The switch in bonding preference on going from Sm^{II} to Sm^{III} (ionic r_8 = 1.41 and 1.22 Å, respectively; r_6 for Sm^{II} = 1.10 Å) seems to parallel the experimental trend for Mg, Ca, Sr, and Ba (ionic r_6 = 0.86, 1.14, 1.32, and 1.49 Å, respectively). It is therefore consistent with Ae−TM and Ln−TM metal−metal bonding being favored by a larger charge/size ratio, as would be expected for predominantly ionic bonding. However, bonding to other Lewis donors present (e.g., THF and (μ-OC)TM η^1-isocarbonyl groups) competes with the metal−metal bonding, as exemplified by the series and $[MgFp_2(THF)]_2$ (**9**, two Mg−Fe bonds), $MgFp_2(THF)_4$ (**8**, two (μ-OC)Fe isocarbonyl bridges), and $[Mg(HMPA)_4][Fp]_2$ (**10**, complete ejection of the Fp^- anion from the coordination sphere).

ASSOCIATED CONTENT

Supporting Information

The Supporting Information is available free of charge on the ACS Publications website at DOI: 10.1021/jacs.5b07866.

General experimental procedures and details of starting materials. Details of the synthesis and characterizing data for new compounds (PDF)

Further details of the diffusion NMR measurements; DFT calculations; and crystal structure determinations, including X-ray data collection and processing parameters and further data (CIF)

Rotatable structure (XYZ)

DOI: 10.1021/jacs.5b07866
J. Am. Chem. Soc. 2015, 137, 12352−12368

AUTHOR INFORMATION

Corresponding Authors

*n.kaltsoyannis@ucl.ac.uk

*philip.mountford@chem.ox.ac.uk

Notes

The authors declare no competing financial interest.

ACKNOWLEDGMENTS

We thank the Leverhulme Trust for support and Corpus Christi College, Oxford, for a junior research fellowship to M.P.B. We also thank University College London for computing resources via the Research Computing "Legion" cluster Legion@UCL and associated services and are grateful for computational resources from the EPSRC's National Service for Computational Chemistry Software, http://www.nsccs.ac.uk. We thank Professor T. D. W. Claridge for assistance with the diffusion NMR studies.

REFERENCES

(1) (a) Liddle, S. T. *Molecular Metal-Metal Bonds: Compounds, Synthesis, Properties*; Wiley: Weinheim, 2015. (b) Bauer, J.; Braunschweig, H.; Dewhurst, R. D. *Chem. Rev.* **2012**, *112*, 4329. (c) Cotton, F. A.; Murillo, C. A.; Walton, R. A. *Multiple Bonds Between Metal Atoms*. 3rd ed.; Springer: New York, 2005.

(2) (a) Li, T.; Schulz, S.; Roesky, P. W. *Chem. Soc. Rev.* **2012**, *41*, 3759. (b) Zhu, Z.; Brynda, M.; Wright, R. J.; Fischer, R. C.; Merrill, W. A.; Rivard, E.; Wolf, R.; Fettinger, J. C.; Olmstead, M. M.; Power, P. P. *J. Am. Chem. Soc.* **2007**, *129*, 10847. (c) Fedushkin, I. L.; Skatova, A. A.; Ketkov, S. Y.; Eremenko, O. V.; Piskunov, A. V.; Fukin, G. K. *Angew. Chem., Int. Ed.* **2007**, *46*, 4302. (d) Grirrane, A.; Resa, I.; Rodriguez, A.; Carmona, E.; Alvarez, E.; Gutierrez-Puebla, E.; Monge, A.; Galindo, A.; del Rio, D.; Andersen, R. A. *J. Am. Chem. Soc.* **2007**, *129*, 693. (e) Wang, Y.; Quillian, B.; Wei, P.; Wang, H.; Yang, X.-J.; Xie, Y.; King, R. B.; Schleyer, P. v. R.; Schaefer, H. F.; Robinson, G. H. *J. Am. Chem. Soc.* **2005**, *127*, 11944. (f) Resa, I.; Carmona, E.; Gutierrez-Puebla, E.; Monge, A. *Science* **2004**, *305*, 1136.

(3) (a) Jones, C.; Mountford, P.; Stasch, A.; Blake, M. P. s-Block Metal-Metal Bonds. In *Molecular Metal–Metal Bonds: Compounds, Synthesis, Properties*; Liddle, S. T., Ed.; Wiley-VCH: Weinheim, 2015; p 23. (b) Stasch, A.; Jones, C. *Dalton Trans.* **2011**, *40*, 5659. (c) Green, S. P.; Jones, C.; Stasch, A. *Science* **2007**, *318*, 1754.

(4) (a) Power, P. P. *Chem. Rev.* **2012**, *112*, 3482–3507. (b) Noor, A.; Wagner, F. R.; Kempe, R. *Angew. Chem., Int. Ed.* **2008**, *47*, 7246. (c) Nguyen, T.; Sutton, A. D.; Brynda, M.; Fettinger, J. C.; Long, G. J.; Power, P. P. *Science* **2005**, *310*, 844.

(5) (a) Oelkers, B.; Kempe, R. Group 3, Lanthanide and Actinide Metal-Metal Bonds. In *Molecular Metal–Metal Bonds: Compounds, Synthesis, Properties*; Liddle, S. T., Ed.; Wiley-VCH: Weinheim, 2015; p 47. (b) Oelkers, B.; Butovskii, M. V.; Kempe, R. *Chem. - Eur. J.* **2012**, *18*, 13566. (c) Gonzalez-Gallardo, S.; Bollermann, T.; Fischer, R.; Murugavel, R. *Chem. Rev.* **2012**, *112*, 3136. (d) Liddle, S. T.; Mills, D. P. *Dalton Trans.* **2009**, 5592. (e) Roesky, P. W. *Dalton Trans.* **2009**, 1887.

(6) (a) Butovskii, M. V.; Oelkers, B.; Bauer, T.; Bakker, J. M.; Bezugly, V.; Wagner, F. R.; Kempe, R. *Chem. - Eur. J.* **2014**, *20*, 2804. (b) Sobaczynski, A. P.; Bauer, T.; Kempe, R. *Organometallics* **2013**, *32*, 1363. (c) Butovskii, M. V.; Tok, O. L.; Bezugly, V.; Wagner, F. R.; Kempe, R. *Angew. Chem., Int. Ed.* **2011**, *50*, 7695. (d) Döring, C.; Dietel, A.-M.; Butovskii, M. V.; Bezugly, V.; Wagner, F. R.; Kempe, R. *Chem. - Eur. J.* **2010**, *16*, 10679. (e) Butovskii, M. V.; Döring, C.; Bezugly, V.; Wagner, F. R.; Grin, Y.; Kempe, R. *Nat. Chem.* **2010**, *2*, 741. (f) Arnold, P. L.; McMaster, J.; Liddle, S. T. *Chem. Commun.* **2009**, 818. (g) Butovskii, M. V.; Tok, O. L.; Wagner, F. R.; Kempe, R. *Angew. Chem., Int. Ed.* **2008**, *47*, 6469. (h) Beletskaya, I. P.; Voskoboynikov, A. Z.; Chuklanova, E. B.; Kirillova, N. I.; Shestakova, A. K.; Parshina, I. N.; Gusev, A. I.; Magomedov, G. K.-I. *J. Am. Chem. Soc.* **1993**, *115*, 3156. (i) Deng, H.; Chun, S.-H.; Florian, P.; Grandinetti, P. J.; Shore, S. G. *Inorg. Chem.* **1996**, *35*, 3891. (j) Deng, H.; Shore, S. G. *J. Am. Chem. Soc.* **1991**, *113*, 8538.

(7) (a) Sanden, T.; Gamer, M. T.; Fagin, A. A.; Chudakova, V. A.; Konchenko, S. N.; Fedushkin, I. L.; Roesky, P. W. *Organometallics* **2012**, *31*, 4331. (b) Fedushkin, I. L.; Lukoyanov, A. N.; Tishkina, A. N.; Maslov, M. O.; Ketkov, S. Y.; Hummert, M. *Organometallics* **2011**, *30*, 3628. (c) Krinsky, J. L.; Minasian, S. G.; Arnold, J. *Inorg. Chem.* **2011**, *50*, 345. (d) Zeckert, K.; Zahn, S.; Kirchner, B. *Chem. Commun.* **2010**, *46*, 2638. (e) Jones, C.; Stasch, A.; Woodul, W. D. *Chem. Commun.* **2009**, 113. (f) Liddle, S. T.; Mills, D. P.; Gardner, B. M.; McMaster, J.; Jones, C.; Woodul, W. D. *Inorg. Chem.* **2009**, *48*, 3520. (g) Arnold, P. L.; Liddle, S. T.; McMaster, J.; Jones, C.; Mills, D. P. *J. Am. Chem. Soc.* **2007**, *129*, 5360. (h) Wiecko, M.; Roesky, P. W. *Organometallics* **2007**, *26*, 4846. (i) Gamer, M. T.; Roesky, P. W.; Konchenko, S. N.; Nava, P.; Ahlrichs, R. *Angew. Chem., Int. Ed.* **2006**, *45*, 4447. (j) Westerhausen, M. *Angew. Chem., Int. Ed. Engl.* **1994**, *33*, 1493. (k) Bochkarev, M. N.; Khramenkov, V. V.; Rad'kov, Y. F.; Zakharov, L. N.; Struchkov, Y. T. *J. Organomet. Chem.* **1991**, *408*, 329.

(8) (a) Ward, A. L.; Lukens, W. W.; Lu, C. C.; Arnold, J. *J. Am. Chem. Soc.* **2014**, *136*, 3647–3654. (b) Napoline, J. W.; Kraft, S. J.; Matson, E. M.; Fanwick, P. E.; Bart, S. C.; Thomas, C. M. *Inorg. Chem.* **2013**, *52*, 12170. (c) Patel, D.; Moro, F.; McMaster, J.; Lewis, W.; Blake, A. J.; Liddle, S. T. *Angew. Chem., Int. Ed.* **2011**, *50*, 10388. (d) Minasian, S. G.; Krinsky, J. L.; Williams, V. A.; Arnold, J. *J. Am. Chem. Soc.* **2008**, *130*, 10086. (e) Liddle, S. T.; McMaster, J.; Mills, D. P.; Blake, A. J.; Jones, C.; Woodul, W. D. *Angew. Chem., Int. Ed.* **2009**, *48*, 1077. (f) Gardner, B. M.; McMaster, J.; Lewis, W.; Liddle, S. T. *Chem. Commun.* **2009**, 2851. (g) Gardner, B. M.; McMaster, J.; Moro, F.; Lewis, W.; Blake, A. J.; Liddle, S. T. *Chem. - Eur. J.* **2011**, *17*, 6909. (h) Nolan, S. P.; Porchia, M.; Marks, T. J. *Organometallics* **1991**, *10*, 1450. (i) Sternal, R. S.; Marks, T. J. *Organometallics* **1987**, *6*, 2621. (j) Sternal, R. S.; Brock, C. P.; Marks, T. J. *J. Am. Chem. Soc.* **1985**, *107*, 8270.

(9) (a) Lalrempuia, R.; Stasch, A.; Jones, C. *Chem. - Asian J.* **2015**, *10*, 447. (b) Bonyhady, S. J.; Jones, C.; Nembenna, S.; Stasch, A.; Edwards, A. J.; McIntyre, G. J. *Chem. - Eur. J.* **2010**, *16*, 938. (c) Krieck, S.; Gorls, H.; Yu, L.; Reiher, M.; Westerhausen, M. *J. Am. Chem. Soc.* **2009**, *131*, 2977. (d) Westerhausen, M.; Gartner, M.; Fischer, R.; Langer, J.; Yu, L.; Reiher, M. *Chem.—Eur. J.* **2007**, *13*, 6292.

(10) For a discussion see reference 3a and leading references therein.

(11) (a) Hicks, J.; Hoyer, C. E.; Moubaraki, B.; Manni, G. L.; Carter, E.; Murphy, D. M.; Murray, K. S.; Gagliardi, L.; Jones, C. *J. Am. Chem. Soc.* **2014**, *136*, 5283. (b) Blake, M. P.; Kaltsoyannis, N.; Mountford, P. *Chem. Commun.* **2013**, *49*, 3315. (c) Ohashi, M.; Matsubara, K.; Iizuka, T.; Suzuki, H. *Angew. Chem., Int. Ed.* **2003**, *42*, 937. (d) Golden, J. T.; Peterson, T. H.; Holland, P. L.; Bergman, R. G.; Andersen, R. A. *J. Am. Chem. Soc.* **1998**, *120*, 223. (e) Kaschube, W.; Pörschke, K.-R.; Angermund, K.; Krüger, C.; Wilke, G. *Chem. Ber.* **1988**, *121*, 1921. (f) Jonas, K.; Koepe, G.; Krüger, C. *Angew. Chem., Int. Ed. Engl.* **1986**, *25*, 923. (g) Davies, S. G.; Green, M. L. H. *J. Chem. Soc., Dalton Trans.* **1978**, 1510. (h) Green, M. L. H.; Luong-Thi, T.; Moser, G. A.; Packer, I.; Pettit, F.; Roe, D. M. *J. Chem. Soc., Dalton Trans.* **1976**, 1988. (i) Green, M. L. H.; Moser, G. A.; Packer, I.; Petit, F.; Forder, R. A.; Prout, K. *J. Chem. Soc., Chem. Commun.* **1974**, 839. (j) Felkin, H.; Knowles, P. J.; Meunier, B.; Mitschler, A.; Ricard, L.; Weiss, R. *J. Chem. Soc., Chem. Commun.* **1974**, 44.

(12) Braunschweig, H.; Gruss, K.; Radacki, K. *Angew. Chem., Int. Ed.* **2009**, *48*, 4239.

(13) Blake, M. P.; Kaltsoyannis, N.; Mountford, P. *J. Am. Chem. Soc.* **2011**, *133*, 15358.

(14) Fletcher, D. A.; McMeeking, R. F.; Parkin, D. *J. Chem. Inf. Model.* **1996**, *36*, 746 The UK Chemical Database Service: CSD version 5.35 updated May 2015.

(15) (a) Gade, L. H. Group 4 Metal-Metal Bonds. In *Molecular Metal-Metal Bonds: Compounds, Synthesis, Properties*, Liddle, S. T., Ed. Wiley-VCH: Weinheim, 2015; pp 73;. (b) Gade, L. H. *Angew. Chem., Int. Ed.* **2000**, *39*, 2658.

(16) Plecnik, C. E.; Liu, S.; Shore, S. G. *Acc. Chem. Res.* **2003**, *36*, 499.

DOI: 10.1021/jacs.5b07866
J. Am. Chem. Soc. 2015, 137, 12352–12368

(17) Heller, J. *Catch-22*. Simon & Schuster: New York, 1961.
(18) Bauer, T.; Wagner, F. R.; Kempe, R. *Chem. - Eur. J.* **2013**, *19*, 8732.
(19) Westerhausen, M. *Coord. Chem. Rev.* **2008**, *252*, 1516.
(20) McVicker, G. B. *Inorg. Chem.* **1975**, *14*, 2087.
(21) Hey-Hawkins, E.; Von Schnering, H. G. *Z. Naturforsch., B: J. Chem. Sci.* **1991**, *46*, 621.
(22) (a) Pannell, K. H.; Jackson, D. *J. Am. Chem. Soc.* **1976**, *98*, 4443. (b) Theys, R. D.; Dudley, M. E.; Hossain, M. M. *Coord. Chem. Rev.* **2009**, *253*, 180.
(23) (a) Jansen, G.; Schubart, M.; Findeis, B.; Gade, L. H.; Scowen, I. J.; McPartlin, M. *J. Am. Chem. Soc.* **1998**, *120*, 7239. (b) Zhao, D.; Ladipo, F. T.; Braddock-Wilking, J.; Brammer, L.; Sherwood, P. *Organometallics* **1996**, *15*, 1441.
(24) (a) Matioszek, D.; Katir, N.; Ladeira, S.; Castel, A. *Organometallics* **2011**, *30*, 2230. (b) Bonello, O.; Jones, C.; Stasch, A.; Woodul, W. D. *Organometallics* **2010**, *29*, 4914. (c) Fedushkin, I. L.; Lukoyanov, A. N.; Tishkina, A. N.; Fukin, G. K.; Lyssenko, K. A.; Hummert, M. *Chem. - Eur. J.* **2010**, *16*, 7563. (d) Wiecko, M.; Roesky, P. W.; Nava, P.; Ahlrichs, R.; Konchenko, S. N. *Chem. Commun.* **2007**, 927. (e) Jones, C.; Mills, D. P.; Platts, J. A.; Rose, R. P. *Inorg. Chem.* **2006**, *45*, 3146.
(25) Cordero, B.; Gomez, V.; Platero-Prats, A. E.; Reves, M.; Echeverria, J.; Cremades, E.; Barragan, F.; Alvarez, S. *Dalton Trans.* **2008**, 2832.
(26) Loubser, C.; Dillen, J. L. M.; Lotz, S. *Polyhedron* **1991**, *10*, 2535.
(27) Brammer, L.; Mareque Rivas, J. C.; Zhao, D. *Inorg. Chem.* **1998**, *37*, 5512.
(28) Tolman, C. A. *Chem. Rev.* **1977**, *77*, 313.
(29) Schumann, H.; Schutte, S.; Kroth, H.-J.; Lentz, D. *Angew. Chem., Int. Ed.* **2004**, *43*, 6208.
(30) Pyykkö, P.; Atsumi, M. *Chem. - Eur. J.* **2009**, *15*, 186.
(31) Shannon, R. D. *Acta Crystallogr., Sect. A: Cryst. Phys., Diffr., Theor. Gen. Crystallogr.* **1976**, *A32*, 751.
(32) Mingos, D. M. P. *Essential Trends in Inorganic Chemistry*. Oxford University Press: Oxford, 1998.
(33) Evans, W. J.; Bloom, I.; Grate, J. W.; Hughes, L. A.; Hunter, W. E.; Atwood, D. A. *Inorg. Chem.* **1985**, *24*, 4620.
(34) (a) Gardner, B. M.; Patel, D.; Cornish, A. D.; McMaster, J.; Lewis, W.; Blake, A. J.; Liddle, S. T. *Chem. - Eur. J.* **2011**, *17*, 11266. (b) Vlaisavljevich, B.; Miró, P.; Cramer, C. J.; Gagliardi, L.; Infante, I.; Liddle, S. T. *Chem. - Eur. J.* **2011**, *17*, 8424. (c) Minasian, S. G.; Krinsky, J. L.; Arnold, J. *Chem. - Eur. J.* **2011**, *17*, 12234.
(35) Elschenbroich, C. *Organometallics*. 3rd ed.; Wiley: Weinheim, 2006.
(36) (a) Ziegler, T.; Rauk, A. *Inorg. Chem.* **1979**, *18*, 1558. (b) Ziegler, T.; Rauk, A. *Inorg. Chem.* **1979**, *18*, 1755.
(37) Bader, R. F. W. *Atoms in Molecules: A Quantum Theory*. Oxford University Press: Oxford, 1990.
(38) Perrin, L.; Clot, E.; Eisenstein, O.; Loch, J.; Crabtree, R. H. *Inorg. Chem.* **2001**, *40*, 5806.
(39) Bianchi, R.; Gervasio, G.; Marabello, D. *Inorg. Chem.* **2000**, *39*, 2360.
(40) Glock, C.; Loh, C.; Gorls, H.; Krieck, S.; Westerhausen, M. *Eur. J. Inorg. Chem.* **2013**, *2013*, 3261.

DOI: 10.1021/jacs.5b07866
J. Am. Chem. Soc. 2015, 137, 12352−12368